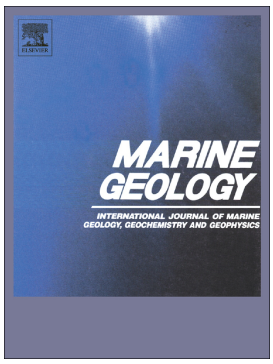

Tectonic evolution, geomorphology and influence of bottom currents along a large submarine canyon system: The São Vicente Canyon (SW Iberian margin)

Cristina S. Serra, Sara Martínez-Loriente, Eulàlia Gràcia, Roger Urgeles, Alexis Vizcaino, Héctor Perea, Rafael Bartolome, Raimon Pallàs, Claudio Lo Iacono, Susana Diez, Juanjo Dañobeitia, Pedro Terrinha, Nevio Zitellini

PII: S0025-3227(20)30107-9

DOI: https://doi.org/10.1016/j.margeo.2020.106219

Reference: MARGO 106219

To appear in: *Marine Geology*

Received date: 10 January 2020

Revised date: 28 April 2020

Accepted date: 30 April 2020

Please cite this article as: C.S. Serra, S. Martínez-Loriente, E. Gràcia, et al., Tectonic evolution, geomorphology and influence of bottom currents along a large submarine canyon system: The São Vicente Canyon (SW Iberian margin), *Marine Geology* (2019), https://doi.org/10.1016/j.margeo.2020.106219

Tectonic evolution, geomorphology and influence of bottom currents along a large submarine canyon system: The São Vicente Canyon (SW Iberian Margin)

Cristina S. Serra[1,2*], Sara Martínez-Loriente[1,3], Eulàlia Gràcia[1], Roger Urgeles[1], Alexis Vizcaino[1], Héctor Perea[1,4], Rafael Bartolome[1], Raimon Pallàs[2], Claudio Lo Iacono[1,5], Susana Diez[6], Juanjo Dañobeitia[6], Pedro Terrinha[7,8] and Nevio Zitellini[9]

[1]*Institut de Ciències del Mar, (CSIC), 08003 Barcelona, Spain*

[2]*Dpt. Geodinàmica de la Terra i l'Oceà, Univ. Barcelona, 08028 Barcelona, Spain*

[3]*Irish Centre for Research in Applied Geosciences, UCD School of Earth Sciences, Dublin 4, Ireland*

[4]*Dept. de Geodinámica, Estratigrafía y paleontología, Facultad de Ciencias Geológicas -Universidad Complutense de Madrid, 28040 Madrid, Spain*

[5]*Marine Geoscience, National Oceanography Centre, Southampton SO14 3ZH, UK*

[6]*Unitat de Tecnologia Marina, UTM-CSIC, 08003 Barcelona, Spain*

[7]*Instituto Português do Mar e da Atmosfera, IPMA, 1749-077 Lisboa, Portugal*

[8]*IDL; Faculdade de Ciências da Universidade de Lisboa, Campo Grande, Edificio C8, Piso 3, 1749-016 Lisbon, Portugal*

[9]*CNR-National Research Council of Italy, ISMAR-Marine Science Institute in Bologna, 40129 Bologna, Italia*

*Corresponding author: csserra@icm.csic.es

Abstract

A multi-scale dataset consisting of multi-beam echo-sounder, 2D multi-channel seismic and sidescan sonar (TOBI) data allows us to identify a large variety of morphologies originating from sedimentary and tectonic processes along the São Vicente Canyon (SVC), which is the largest submarine canyon developed in the external part of the Gulf of Cadiz. The SVC is located in one of the most seismogenic areas of Western Europe.

The convergence between the Eurasian and African plates has controlled the formation and evolution of the canyon. The SVC is tectonically controlled by three main thrust faults: the Marquês de Pombal Fault, the São Vicente Fault and the Horseshoe Fault. No major rivers feed sediment to the canyon head, but the main sediment source is related to the dismantling of canyon flanks and the MOW (Mediterranean Overflow Water). This current contributes sediments by two different processes: a) conturites deposition at the head and flanks of the SVC that periodically fail into the canyon; and b) the coarser-grained and denser sediment of the MOW might be trapped at the head of the canyon and could develops into hyperpycnal flows . The SVC is characterized by retrogressive erosion being submarine landslide deposits and scars the main seafloor morphologies. The tectonic and stratigraphic interpretation of seismic profiles indicate that the SVC is a clear example of a diachronous and segmented canyon developed since the Late Miocene in an area of present-day active plate tectonics. This study investigates the interaction between active tectonics, the dynamics of submarine canyons and the resulting geomorphologies.

Keywords: submarine canyons, thrust faults, bottom currents, sedimentary pathways, sidescan-sonar, seismic reflection.

1. Introduction

Submarine canyons are major sediment pathways that link shallow continental shelf areas to the deep sea. They play an important global role in the development of continental margins. Submarine canyons not only act as conduits for sediments, but also they play a role as main transport corridor for associated nutrients, organic carbon, litter and pollutants travelling from the continental shelves to the abyssal plains (Amblas et al., 2012; Lastras et al., 2009; Micallef et al., 2014; Pierdomenico et al., 2019; Shepard, 1981). Erosion and sediment re-mobilization induced by sediment-laden gravity flows

(e.g. turbidity currents), which travel from the head and flanks of the canyon towards the deep oceanic basins (Lewis and Barnes, 1999), are the main factors in the generation of submarine canyons. Temporary sediment accumulations near the canyon head may become unstable due to a number of factors, such as over-steepening, earthquake-triggered deformation, sediment liquefaction and basal erosion of canyon flanks (Arzola et al., 2008). However, other flows such as hyperpycnal flows that generated submarine slope failures at the canyon head, and dense shelf water cascading (Canals et al., 2006; Palanques et al., 2006; Puig et al., 2014) may cause erosion and transport of large sediment volumes along the entire canyon.

The onset of canyon development and its subsequent evolution is determined by a number of factors, including sediment sources and the resulting sedimentary and erosive processes that shape the canyon floor and their flanks (Amblas et al., 2011). Sediments may derive from fluvial sources (i.e. most existing canyons are directly fed by rivers, particularly during sea level low-stands) (Mauffrey et al., 2017) or along-shore currents (Piper and Normark, 2009). In addition, structural control has also been proposed (Micallef et al., 2014).

The São Vicente Canyon (SVC) is the largest submarine canyon in the SW Iberian margin (Fig. 1), transporting sediment from the shelf break (~200 m water depth, where the SVC head is located) to the Horseshoe Abyssal Plain (4900 m at the SVC mouth), although no major river feeds sediment to its head. The SVC is located in a convergent setting placed between the Eurasian and African plates, which greatly control its dynamics. In this work, we use a multi-scale dataset and different analysis techniques to describe the tectonic, sedimentary and erosional processes linked to the canyon, and to propose a conceptual model to discuss the emplacement, age and evolution of the SVC.

This study improves the knowledge on the origin and interplay between active tectonics, the dynamics of submarine canyons, and the resulting geomorphologies.

2. Geological setting

The SVC is located on the external part of the Gulf of Cadiz (SW Portuguese margin), along the Eurasian-African plate boundary. Present-day tectonic deformation is mainly driven by NW-SE trending convergence, with an estimated velocity of 3.8-5.6 mm a^{-1} (Neres et al., 2016; Nocquet and Calais, 2004) (Fig. 1).

The SW Iberian margin has undergone a complex geodynamic evolution that includes three rifting phases during the Mesozoic (i.e., the opening of the Central Atlantic and the western Alpine-Tethys spreading system in the Early Jurassic, followed by the first stage of the North Atlantic opening in the Lower Cretaceous) and a Neogene-to-present-day convergence (Martínez-Loriente et al., 2014; Sallarès et al., 2013, 2011). The latest Neogene convergence stage, mainly trending NNW-SSE (Schettino and Turco, 2009), resulted in the emplacement of large allochthonous masses during the Tortonian (Gràcia et al., 2003a; Iribarren et al., 2007). As a result of the Neogene collision, Mesozoic extensional faults were reactivated and new fault systems appeared in weakened areas. There are two main families of active faults: a) NE-SW trending reverse faults, and b) WNW-ESE trending dextral strike-slip faults (Gràcia et al., 2003a; Gràcia et al., 2003b; Martínez-Loriente et al., 2018, 2014, 2013; Terrinha et al., 2009, 2003) (Fig. 1).

The SW Iberia is an area of low to intermediate magnitude earthquakes ($M_w < 5.5$), occasionally punctuated by high-magnitude seismic activity (Buforn et al., 1995; Martínez-Loriente et al., 2018, 2013; Stich et al., 2005) (Fig. 1), with focal mechanisms indicating compressional stress and/or strike-slip regime (Buforn et al., 1995; Stich et al., 2005). This area is also the source of the largest historical and instrumental

earthquakes in Western Europe, including the earthquakes and tsunamis of the 26 January 1531 Tagus Estuary tsunami (MSK = X), the 27 December 1722 Tavira tsunami, (M_w 6.5) and the 1 November 1755 Lisbon earthquake ($M_w \geq 8.5$) (Baptista and Miranda, 2009) events (Fig. 1). This last earthquake caused extensive destruction in Portugal, southern Spain and western Morocco (Baptista and Miranda, 2009; Barkan et al., 2009; Gràcia et al., 2010). In recent times, earthquakes of considerable magnitude have nucleated in the study area on the 28 February 1969 (M_w 7.9-8.0), 12 February 2007 (M_w 6.0), and 17 December 2009 (M_w 5.5) (Stich et al., 2006; Lozano et al., 2019) (Fig.1).

The physiography of the Portuguese margin is characterized by the presence of numerous large submarine canyons, such as the Faro, Portimão and Lagos canyons in the south (Mulder et al., 2006; Vizcaino et al., 2005a), and the Cascais, Lisbon, Setúbal and Nazaré canyons in the west of Portugal (Arzola et al., 2008; Lastras et al., 2009; Oliveira et al., 2007; Terrinha et al., 2019) (Fig. 1). The oceanic circulation of the Gulf of Cadiz is dominated by the MOW (Mediterranean Outflow Water) (Fig. 1). The MOW is a salty, warm and poorly oxygenated submarine current that flows from the Strait of Gibraltar towards the Atlantic following the slope and the Portuguese continental shelf (Hernández-Molina et al., 2003). Along its pathway, the MOW loses velocity and increases in depth. At the head of the SVC, the MOW generates associated sedimentary deposits such as contourites (Hernández-Molina et al., 2013).

The SVC extends from Cape São Vicente on the Portuguese coast to the Horseshoe Abyssal Plain, bounded by the Sagres Plateau and the Horseshoe Fault to the east, and by the Marquês de Pombal fault block to the west (Fig. 1). The SVC is located in a syncline fold in between two prominent anticlines (i.e., the Marques de Pombal block and the Sagres Palteau) (Vizcaino et al., 2005b; Zitellini et al., 2001; Pereira and Alves,

2013) and is mainly dominated by the NE-SW-trending reverse Horseshoe Fault (Martínez-Loriente et al., 2018) (Fig. 1). Alternatively, some authors propose that the SVC is linked with the prolongation offshore of the Messejana–Plasencia Fault Zone (Pereira and Alves, 2013). The sedimentary inputs to the SVC are mainly fed by along-the-shelf sediment transport sources (i.e., the MOW) (Mastbergen and Van Den Berg, 2003). Most of the sediments travelling along the SVC are deposited in the Horseshoe Abyssal Plain (Gràcia et al., 2010).

3. Data and Methods

The multi-scale dataset used in this work includes existing swath-bathymetry, sidescan sonar (TOBI) and multi-channel seismic (MCS) data (Fig. 2). Swath bathymetric data in the Gulf of Cadiz was acquired during 20 different marine cruises, from 2001 to 2009, using different multibeam echosounder systems. Ten European contributors collaborated to complete the bathymetric map of the Gulf of Cadiz, the "SWIM" compilation published by Zitellini et al. (2009) (Figs. 1, 2). Sidescan sonar data (Figs. 2, 5, 6, 7) were acquired on board the RV *Hesperides* during the "HITS" (*High Resolution Imaging of Tsunamigenic Structures of the Southern Iberian Margins*) survey (Gràcia et al., 2003a; Gràcia et al., 2006) by using the TOBI (Towed Ocean Bottom Instrument) side-scan sonar vehicle (Flewellen et al., 1993). The sidescan sonar system used a 30 kHz sonar frequency on a vehicle towed 200 to 500 m above the sea-floor to generate images with 6 m along-track resolution (Blondel and Murton, 1997). The data used for this study consisted of four 6-km-wide parallel tracks covering most of the São Vicente Canyon. In this study, swath-bathymetry and side-scan sonar data were analysed using the ArcGIS 10 commercial package.

The sinuosity index of the SVC has been calculated using the ratio of curvilinear to straight length (Leopold and Wolman, 1957). The volume of the eroded material by the

SVC has been determined by calculating the difference in elevation between a spline-smoothed grid where the canyon topography was removed, therefore simulating the slope without canyon incision (Fig. S1) and the grid of the actual slope (Fig. S1).

The Multi-channel seismic (MCS) data available for this study consists of 17 profiles acquired with different configurations during different marine surveys (Fig. 2). The "AR" profiles, belonging to the 1992 ARRIFANO cruise, were acquired with the R/V OGS EXPLORA (Zitellini et al., 1999). This survey used an airgun array of 32 guns with a total capacity of 4880 cubic inches (c.i.) and a 3-km-long streamer with 120 channels and 50 m shooting interval (Zitellini et al., 1999). The AR data was processed with spiking deconvolution, spherical divergence correction, NMO correction, finite-difference wave-equation migration and time variant band-pass frequency filter (Zitellini et al., 2009). The "BS" profiles from the BIGSETS survey were acquired on board the R/V URANIA during November 1998 (Zitellini et al., 2001). The seismic source consisted of an array of two GI-guns with a total volume ranging from 150 to 465 c.i. The seismic signal was recorded with a 1.2 km-long streamer of 48 channels and 25, 37 and 50 m shooting interval (Zitellini et al., 2004, 2001). The processing of BIGSETS MCS data consisted in spiking deconvolution, velocity analysis every 2.5 km, NMO correction, spherical divergence correction and finite-difference wave-equation time migration using stacking velocities reduced by 10% (Zitellini et al., 2004). The "VOL" profiles correspond to the 2002 VOLTAIRE survey carried out on board the R/V URANIA. In this survey, 2 GI guns totalling 210 c.i. were shot every 50 m and a 600 m-long, 48 channel streamer was used (Terrinha et al., 2009). The MCS VOLTAIRE dataset was processed with trace editing, shot delay removal, amplitude recovery, predictive deconvolution, velocity analysis every 200 CMPs, NMO correction, stack, bandpass-frequency filtering and time migration using stacking

velocities reduced by 10%. The analysis and geological interpretation of the 17 MCS profiles used in this study were carried out using the "IHS Kingdom Suite" seismic interpretation software.

In this work, the seismostratigraphic units defined by Martínez-Loriente et al. (2013) were correlated throughout the seismic network of profiles shown in Figure 2 (see supplementary material Fig. S2). These units were defined based on the DSDP (Deep Sea Drilling Project) Site 135 (Hayes et al., 1972) and correlated with those previously defined in the area (Tortella et al., 1997; Hayward et al., 1999; Medialdea et al., 2004). In addition, the tectonic and stratigraphic analysis carried out by Martínez-Loriente et al. (2018) along three MCS profiles crossing the mouth of the SVC has been used in this work as a reference. Hernández-Molina et al. (2015) defined four Quaternary subunits based on IODP (International Ocean Discovery Program) Site 339 results (Hernández-Molina et al., 2013). The lack of seismic data connecting the Site 339 to the study area, prevents a confident age assignment to the four unconformities identified within the youngest unit in the seismic dataset used in this work (i.e., subunit Ia; see Supplementary Material Figs. S2, S3).

4. Results

4.1. Geomorphology and acoustic character of the São Vicente Canyon

The SVC is a 157 km-long canyon connecting the continental shelf, at 200 m water depth, to the Horseshoe Abyssal Plain at 4900 m water depth (Figs. 1, 2). The sinuosity (winding), is 1.12 and its average axial slope is 1.8^{o} (Fig. 3). The path of the SVC is characterized by several changes in orientation and slope. Accordingly, the canyon has been divided in three main sections, from north to south: 1) the upper section (canyon head) is 60 km-long, trends N50, and extends from the continental shelf from water depth of 200 m to 3200 m (Fig. 3a); 2) the central section is 54 km–long, trends N20 in

the northern part and N160 in the southern end, covering the area located between 3200 m and 4400 m water depth (Fig. 3b); and 3) the lower section is 43 km-long, trends N30 (parallel to the Horseshoe Fault), and extends from 4400 m to 4900 m water depth towards the canyon mouth in the Horseshoe Abyssal Plain (Fig. 3c).

A significant characteristic of the SVC is that the longitudinal bathymetric profile of the canyon axis (Fig. 4d) presents a rectilinear morphology with a rather constant slope and, therefore, does not appear to be in equilibrium. Generally, bathymetric profiles that are in equilibrium, similarly to rivers on land, show a logarithmic longitudinal-profile (Amblas et al., 2012). However, the longitudinal profile of the SVC shows a rather linear morphology (Fig. 4d) although the flanks are clearly asymmetric and its height and slope vary along the canyon (profiles across the canyon in Figs. 4a, c) (Fig. 3).On the TOBI mosaic, the canyon floor and the lower part of the flanks display heterogeneous high-backscatter acoustic facies (i.e., shown as white and light grey in Figs. 5, 7). In contrast, the canyon flanks and part of the hanging-wall blocks of the Marquês de Pombal Fault (MPF), Horseshoe Fault (HF) and São Vicente Fault (SVF) outside the canyon, are characterized by homogenous dark grey to black colour (i.e., low-acoustic backscatter). The uppermost head-scarps of the flanks in the upper and central sections are homogeneous showing high acoustic backscatter facies.

4.1.1. The upper section of the SVC

The SVC head shows a semi-circular shape cut by three main tributary canyons that converge at 36°59'N (2000 m water depth) (Figs. 2, 3a). At this location, the flanks steepen and the V-shaped thalweg becomes narrower (3 km) (Figs. 3a, 4a). Along the canyon, the slope is roughly constant at 1.02º (Fig. 3a). In this section of the canyon the flanks are characterized by gradients ranging from 9.7º to 26.6º, and a rugged topography. The flanks present a network of rectilinear gullies (rectilinear erosive

landforms usually generated in land that has been remobilized) topped by semi-circular-shape erosional scarps (from 1 to10 kms of diameter) and minor flow pathways (maximum slope lines that can channel flows) that are oriented subparallel to the maximum slope direction and their gradients reach up to 24º (Fig. 3a).

The slope diagram (Fig.3a), the topographic profiles (Fig. 4a) and the acoustic backscatter signal (Fig.5) indicate that the NW flank of the canyon is rougher than the SE flank. Although both flanks show a number of gullies and other minor flow pathways, these are more abundant on the NW flank. The gullies and minor flow pathways (13-14 km-length) appear more incised in the SE flank than in the NW one (Figs. 2, 3, 4d), as the rocky substrate outcrops on the lower part of the SE flank.

The scars are about 1-4 km-wide on both flanks. However, the SE flank shows a single generation of scars, whereas in the NW flank there is evidence for at least two generations of scars. The first generation is located on the uppermost part of the NW flank. The second generation is longer and develops at mid-elevation, disrupting the minor flow pathways from the first generation of scars. The scars on both flanks, but particularly those of the NW flank, are characterized by submarine landslide deposits (up to 5 km-long and 4 km-wide) (Fig. 5).

The most striking feature in the TOBI mosaic is the ENE-WSW trending high-backscatter band, corresponding to the canyon floor (Fig. 5). The acoustic character of the canyon floor is highly heterogeneous, and shows the following features: a) multiple channels along the axis; b) grooves > 1 km-long, pervasive lineaments parallel to the canyon axis carved by sediment transport, of low to medium backscatter areas (grey to light-grey colours); c) sediment accumulation, areas of very-high backscatter along the axis ; d) stratification, low backscatter lineaments showing acoustic shadows on the

lower part of the eastern flank; and e) old terrace, low-backscatter semi-circular area with gentle slope, located on the internal side of a meander attached to the canyon east flank (area in green in Fig. 5b).

4.1.2. The central section of the SVC

Along this section, the canyon axis shows an average slope of 1.02º, whereas its flanks show slopes steeper than 26.6º on the upper part, which gradually decreases southward to 14º (Fig. 3). In the middle of this section, the canyon cross section progressively changes from V-shaped to U-shaped (Figs. 3b, 4b). On the upper part of this central section, the canyon is incised 1000 m on the west flank and 800 m on the eastern one (Fig. 4b). Moving south along the canyon, these values decrease to less than 500 m on the west flank and 300 m at the east one.

Three main tributary canyons converging towards the main canyon can be recognized on the eastern flank of the slope by medium-high backscatter values in the TOBI mosaic (Figs. 3b, 6). The canyon located further north is oriented E-W, whereas the other two canyons are oriented NE-SW and NW-SE respectively, being the three >15 km-long. Both flanks of this section show evidence for stratification, middle to low backscatter lineaments along the canyon and large scars, although less abundant than in the upper section. Some of these scars have associated submarine landslide deposits in the TOBI mosaic. The largest submarine landslide deposit located in the north of this section, is associated to a semi-circular scar of ~ 3 km in diameter and is characterized by > 0.5 km-long high-backscatter patches. Long scars, such as those located on the central section of the NW flank are elongated (> 4 km-long) and characterized by low backscatter.

The canyon floor of this section shows several features similar to those described along the upper section of the canyon (Figs. 5, 6), including: a) a middle-grey backscatter signal that corresponds to the tributary canyons; b) grooves (erosive structures) that particularly stand out in areas of very high backscatter within the canyon floor (i.e., rock outcrops); c) high backscatter areas (light blue areas in the Fig. 6) along the canyon axis and canyon west flank that correspond to sediment accumulations; and d) scours (semi-circular negative relief perpendicular to the flow direction), which may attain a diameter of ~2 km and an elevation of 200 m (namely "steps" in the longitudinal profile on Figs. 3b, 4d and "scours" in Fig.6).

4.1.3. The lower section of the SVC

In this area, the SVC displays a wide U-shaped valley with a 7-km-wide flat canyon floor, low slope axis of 0.9º (Fig. 3c) and low angle flanks (mean slope less than 14º) in comparison to the upper and central canyon sections (Figs. 3, 4). The slope of the western flank flattens to the south towards the Horseshoe Abyssal Plain, whereas the slope of the eastern flank increases, reaching mean values of 16.7º and locally up to 26.6º (Fig. 3c). In this lower section, both the SW flank and the Horseshoe Abyssal Plain display a homogeneous low-backscatter facies and the SW flank presents a large number of canyon-parallel lineaments (stratification).

In the TOBI mosaic (Fig. 7), the canyon floor shows high-backscatter facies that progressively decrease towards the south (Martínez-Loriente et al., 2018). In this section, the canyon does not show a well-developed channel, rather it fades into the Horseshoe Abyssal Plain. The main features in this area include: a) high backscatter patches (probably outcrops), b) canyon-parallel, pervasive grooving (0.5-1 km-length) at the north-eastern part of the canyon floor, and c) low backscatter, 1 km-long comet-like, irregular scours along the main channel.

4.2. Seismo-stratigraphy of the São Vicente Canyon

Seismic horizons have been interpreted based on previous chronostratigraphic information (Fig. S2) (Hayes et al., 1972; Hernández-Molina et al., 2015; Martínez-Loriente et al., 2018, 2013). They have been correlated through the network of vintage and recent MCS profiles, and include the following units: Plio-Quaternary (Ia), Middle Miocene - Pliocene (Ib), Horseshoe gravitational unit (HGU-Ic), Upper Oligocene - Middle Miocene (Id), Upper Cretaceous - Early Eocene (II), Cretaceous (III), Lower Cretaceous (IV), Upper Jurassic (V) and basement (VI) (Fig. 8).

4.2.1. Pliocene-Quaternary (Ia)

Unit Ia is characterized by middle frequency and middle amplitude continuous reflectors. This unit shows lateral continuity and is interrupted near the SVC, which completely erodes the Plio-Quaternary unit in the upper and central sections of the canyon axis (Figs. 8a, 8b). On the canyon flanks, gully incision and tributary canyons erode the uppermost part of this unit (Fig. 8a). The maximum thickness of unit Ia is 1.2s TWTT (Two Way Travel Time) in the upper section of the canyon, which progressively decreases to 0.1s TWTT towards the lower section. In the upper section of the SVC, mainly on the SE flank, contourite geometries can be distinguished (low-aspect, lenticular sedimentary bodies). Within this unit, we identify four discontinuities that may correspond to Late Quaternary (LQD), Mid Pleistocene (MPD), Early Quaternary (EQD) and Late Pliocene (LPD) discontinuities (Figs. S2, S3) described by Hernández-Molina et al. (2015, 2013) based on the IODP Site U1391 (Fig.1).

4.2.2. Middle Miocene-Pliocene (Ib)

Unit Ib is characterized by middle frequency, middle amplitude and continuous reflectors. The thickness of this unit is variable along and across the SVC (Fig. 8), with a maximum thickness of 0.7s TWTT below the canyon axis in the lower section, that

progressively thins towards the flanks. This unit shows onlaps towards the Marquês de Pombal anticline fold and also towards the Horseshoe Fault hanging-wall block (Fig. 8d), so we can distinguish multiple progressive unconformities in the central and lower sections (Figs. 8b, S3). The incision of the canyon causes the total erosion of Unit Ib on the SVC axis of the upper section, whereas is only partially eroded in the central section. Both top and base of Unit Ib are unconformities.

4.2.3. Horseshoe Gravitational Unit (HGU-Ic)

The Horseshoe Gravitational Unit (HGU-Ic) is a wedge-shaped allochthonous body formed by stacked debris-flow that originates from the westward migration of the Gulf of Cadiz Imbricated Wedge (GCIW) and was emplaced during the Upper Miocene (Tortonian) (Gràcia et al., 2003b; Iribarren et al., 2007; Torelli et al., 1997) (Figs. 8c, 8d). The HGU is characterized by high-amplitude chaotic seismic facies with numerous diffractions and hyperbolic reflections. Only a few internal reflectors can be identified. The top and bottom are defined by unconformities (Figs. 8c, 8d). The HGU fills the Horseshoe Valley and the Horseshoe Abyssal Plain, where it pinches out toward the edges of the valley (Martínez-Loriente et al., 2013). Therefore, the HGU can only be identified at the lower section of the canyon, where it reaches a maximum thickness of 1.3 s TWTT. In this section, the HGU partially or totally eroded the underlying Unit Id.

4.2.4. Upper Oligocene-Middle Miocene (Id)

Unit Id is characterized by high-amplitude and low-frequency continuous reflectors. In the upper and central sections of the canyon, Unit Id lies directly below Unit Ib and reaches a maximum thickness of 0.5s TWTT (Fig. 8a). In contrast, in the lower section of the SVC Unit Id lies below the HGU, which partially eroded its top. In this section, the top corresponds to an erosive surface generated by excavation and erosion during the emplacement of the HGU.

4.2.5. Upper Cretaceous-Lower Eocene (II) and Cretaceous (III)

The seismic facies of Units II and III show similar characteristics (Fig. 8). Both have low-frequency and high-amplitude continuous reflectors. The contacts between both units and underlying unit (IV) are concordant. The top of Unit II is composed by a prominent unconformity marked by a high-amplitude reflector that corresponds to a regional sedimentary hiatus from Lower Eocene to Upper Oligocene (Hayes et al., 1972; Martínez-Loriente et al., 2013). Both units onlap the top of the basement (Figs. 8a, 8b). Their thickness is relatively uniform with a maximum value for Unit II of 0.45s TWTT and 0.4s TWTT for Unit III that reached the hanging wall of the Marquês de Pombal Fault. The minimum thickness for Unit II is 0.1s TWTT below the HGU in the lower section of the canyon (Figs. 8c, 8d), and of 0.2s TWTT for Unit III below the SVC at the central section (Fig. 8b). These units infill graben structures of the basement generated as a result of Mesozoic rifting (Martínez-Loriente et al., 2018).

4.2.6. Lower Cretaceous (IV) and Upper Jurassic (V)

The Lower Cretaceous Unit IV and Upper Jurassic Unit V show semi-transparent and transparent seismic facies with low frequency and low amplitude reflectors (Fig. 8). The contact between these units is concordant and can be identified by parallel reflectors onlapping the top of basement highs (Figs. 8a, 8b, 8d). Unit IV reaches a maximum thickness of 0.5s at the hanging wall of the Marquês de Pombal Fault. Unit V directly overlies the basement (i.e. discordant contact) and fills pre-existent half-graben depressions (Fig. 8d). Accordingly, the thickness of Unit V is highly variable, reaching a maximum value of 0.7 s (TWTT) at the lower section of the canyon (Figs. 8c, 8d).

4.2.7. Basement (VI)

The Basement (Unit VI) is interpreted as composed of: a) thinned continental crust in the area of the SVC, Sagres Plateau and the hanging wall of the Marquês de Pombal

Fault Block; b) oceanic crust at the southern half of the lower section of the SVC; and c) serpentinized exhumed mantle at the footwall of the Marquês de Pombal Block (Martinez-Loriente et al., 2014). This heterogeneous composition results in differences on the tectonic architecture of the basement. In the upper and central sections of the SVC, as well as in the MPF block, the MCS profiles reveal tilted basement blocks bounded by large, old normal faults (Figs. 8a, 8b, 8d). In contrast, at the Infante Don Henrique Basin the basement structure is completely different, and peridotite ridges have been identified (Fig. 8d).

4.3. Tectonic structures across and along the São Vicente Canyon

The strata across the SVC are folded by two anticlines bounding a synclinal (Figs. 8c, 8d), partially eroded by the incision of the SVC. The synclinal and anticlinal folds are more pronounced and well-defined in the lower section of the canyon, whereas their morphology is attenuated towards the upper section (Fig. 8).

The anticline located on the western flank of the canyon is controlled by the west-verging monocline thrust Marques de Pombal Fault (MPF) (Fig. 8d) and corresponds to the hanging wall of this active reverse fault (Gràcia et al., 2003a, 2010). The MCS profiles (Fig. 8d) show that the sedimentary sequence rises and tilts towards the SVC axis. The eastern flank of the upper section of the SVC seems to be controlled by the São Vicente Fault (SVF). The west-verging SVF is an NNE-SSO trending thrust that affects all the seismo-stratigraphic units until the seafloor (Ia) (Fig. 8a). Towards the SSW, the SVF becomes a blind-thrust along the canyon axis, which progressively attenuates and disappears (Fig. 8b).

The lower section of the SVC (Fig. 8c, 8d) is dominated by the presence of the west-verging Horseshoe Fault (HF), which is also oriented parallel to the canyon axis trending NE-SW. In this section, the south-eastern flank of the canyon corresponds to

the hanging-wall block of the HF, whereas the canyon floor corresponds to the footwall block. Minor folds are observed in the hanging-wall block near the HF as a fault-propagation-fold (Figs. 8c, 8d). Flexure at the frontal part of the HF thrust generates accommodation space in the footwall, which is progressively filled by sediments transported downstream in the canyon. The HF can be easily identified in the MCS profiles (Figs. 8c, 8d), as well as in the TOBI mosaic (Fig. 7). In the lower section of the canyon, the HF cuts and displaces the entire seismo-stratigraphic sequence (Fig. 8c) (Martínez-Loriente et al., 2018). However, in the lower part of the SVC central section, the HF only cuts the sedimentary cover until the HGU (Tortonian age) and folds the uppermost units, acting as an active blind-thrust (Fig. 8d). In the middle part of the central section of the SVC, the HF cannot be identified neither in the MCS profiles nor in the TOBI mosaic (Figs. 7, 8b) (Martínez-Loriente et al., 2018).

5. Discussion

5.1. Sedimentary processes along the São Vicente Canyon

The highly variable TOBI backscatter evidences Present activity of the canyon. If the identified sedimentary morphologies were relict structures, a thin layer of hemipelagic sediment would homogenize the backscatter while preserving the morphology. Therefore, the TOBI mosaics show that the SVC is a significantly active pathway for sediment transport. Combining the TOBI mosaics and the morphological characteristics of the canyon reveals a predominance of submarine mass-wasting and erosive processes can be envisaged (Figs. 3, 5, 6, 7). These processes are widespread in the canyon flanks characterized by homogenous light-grey colours to low backscatter with dark grey acoustic facies. The retrogressive erosion is prevalent in the upper section of the canyon, with steep slopes favouring the incision of gullies along the canyon walls. These gullies often are topped by circular head-scarps where retrogressive erosion

occurs. These landslide scars are often coalescent and form a sinuous array of unstable features following the main canyon path. Erosion is practically non-existent in the lower section of the SVC (Fig. 3).

Of relevance is the NW flank of the SVC, characterized by a large number of submarine landslides deposits and two generations of landslide scars (Figs. 5, 6). The lower landslide scars postdate the upper landslide scars, in contrast with the overall retrogressive and erosional setting of the canyon. The lower landslide scars (i.e., the second generation) suggest a recent rearrangement of the NW flank. Such rearrangement may result from changes in the base level of the SVC, which tries to come closer to a new equilibrium. In support of this hypothesis most of the deposits associated with the upper landslide scars cannot be recognized as they have been likely eroded. Conversely, the deposits associated with the lower landslide scars can be identified and have not yet been remobilized. The NW flank is located at the hanging wall of the Marquês de Pombal Fault (Fig. 8a), that acts as a barrier and hinders the progression of the axial canyon incision. Mass- wasting processes seem to be particularly active in the NW flank of the canyon, although the length of the flank is shorter and slope gradients are gentler than those in the SE flank. One of the most seismically active areas of the SW Iberian margin is the SVC (Fig. 1), where the so-called São Vicente earthquake cluster nucleates (Geissler et al., 2010; Grevemeyer et al., 2017; Stich et al., 2005). Some authors suggest that the MPF is the tectonic source of the SVC cluster, which nucleates along the canyon at 20-40 km depth (Geissler et al., 2010; Grevemeyer et al., 2017; Martínez-Loriente et al., 2018; Silva et al., 2017). Consequently, seismicity is of special relevance to the occurrence of submarine mass movements in the SVC. The slope of the canyon axis significantly decreases in the lower section of the canyon, where submarine mass movements and turbidity currents

also reduce velocity and erosive capacity (Fig. 3). In this section, erosive structures are almost non-existent and the canyon shows a broad U-shaped profile, also suggesting that there is a change in the dynamics of the canyon and a reduction in erosive capacity.

The high backscatter values in the TOBI mosaic along the canyon thalweg indicate the sediment accumulation of gravel and sand (coarse-grained deposits) (Blondel and Murton, 1997), which provide evidence of the high-energy sediment transport activity along the canyon floor (Figs. 5-7). The accumulation of gravels and sands is scarce and discontinuous and can probably attest to the presence of lag-deposits from sediment gravity flows periodically funnelled along the canyon. The medium-high backscatter values of the three main tributary canyons may suggest current activity. If the tributary canyons were inactive, they would be covered by a thin layer of hemipelagic sediments and their backscatter would be rather low.

Finally, we also recognize erosive bedforms (i.e., grooves and scours) along the central section of canyon thalweg. Scours form semi-circular steps (stepped scours or cyclic steps, which can be erosive, depositional or mixed) perpendicular to the canyon axis (Fig. 4d) partially filled by coarse-grained sediment, as observed in the high-backscatter areas in the TOBI sidescan sonar mosaic (Fig. 6). Stepped scours (upstream-migrating bed-forms), have been interpreted to result from supercritical turbidity currents (Covault et al., 2017) (Figs. 5,6). Migration and growth of these cyclic steps takes place when the higher-density basal layer of the hyperpycnal flows interacts with the seabed triggering a hydraulic jump downstream of the base of the step (Hughes Clarke, 2016). Masson et al. (2004) suggested that this type of scour formation requires minimum current speeds between 1.0 and 2.5 m/s.

5.2. Sediment sources of the São Vicente Canyon

One of the main characteristics of the SVC is that there is no significant fluvial system onshore that could feed sediments to the canyon head (Fig. 1). The main rivers close to the SVC are the Sado River (located 140 km to the north) and the Guadiana River (located 170 km to the east). Both rivers have an adjacent submarine canyon system that trap and distribute their sediments. Therefore, the direct contribution of sediments from the continent to the SVC is relatively low. Thus, the question is, being the canyon disconnected from the onshore main drainages, which are the mechanisms that provide sediments to maintain it active and growing?

Isochore maps show that sediments were mainly accumulated in the central and lower sections of the SVC since the Middle Miocene (Fig. 9c), apparently related to the uplift of the HF hanging wall block and the generation of depositional space in the subsiding footwall block. It seems plausible to consider that the main sediment sources along the SVC are the materials provided by the erosion of canyon flanks through gullies, tributary canyons and submarine mass movements that generate submarine landslide deposits, which are abundant in the upper and central sections of the canyon. Arzola et al. (2008) also proposed similar processes of flanks dismantling for other canyon systems along the Portuguese coast, such as the Nazaré and Setúbal canyons. The total volume eroded by the SVC is 1219 km^3 (Fig. S1).

Nevertheless, there could also be secondary sediment sources feeding both the main SVC and their three tributary canyons. The submarine canyons developed along the Portuguese coast incise the continental shelf (the SVC at the shelf break) and work as traps for sediment transported by bottom currents along the shelf and upper-slope. This is particularly significant in the oceanographic framework of the Gulf of Cadiz, with a complex environment dominated by the Mediterranean Outflow Water (MOW) (Fig. 1). Along its pathway from the Straits of Gibraltar towards the West Iberian Margin, the

MOW decreases in velocity, temperature and salinity (Hernández-Molina et al., 2015). This favours the sedimentary deposits (i.e., contourites) at the head and flanks of the canyons such as the SVC (Hernández-Molina et al., 2003) (Figs. 1, 8a, 8b). The contourites on the upper section of the SVC are deposited in water depths up to 1400 m. At this depth, the sediment transported by the MOW is sand-rich (Hernández-Molina et al., 2015). The TOBI images show coarse-grained sedimentary deposits in the upper and central sections of the SVC that could have been partially deposited by the MOW. Thus, the SVC acts as a sediment trap. The coarser-grained and denser sediment of the MOW is trapped at the head of the canyon, which could eventually evolve into hyperpycnal flows that would down into the canyon and could form steps at the canyon bed. The relatively high seismicity of the area (Fig. 1) triggers periodic failure of sediments accumulated at the edge or within the canyon, which are subsequently transported along the SVC to the Horseshoe Abyssal Plain, as previously described.

5.3. Timing of formation and evolution of the São Vicente Canyon and neighboring areas

The SVC is located in a syncline between two reverse fault-controlled anticlines related to the SVF, HF and MPF thrust faults, which suggests a strong structural control on its development (Figs. 1, 8, 9, 10). Their trend (NE-SW) is compatible with the present-day African-Eurasian plate convergence (NW-SE) (Martínez-Loriente et al., 2013, 2018). Our multidisciplinary dataset gives us some insights about the timing of formation and evolution of these reverse faults and neighbouring areas.

The Upper Cretaceous to Early Eocene period (Unit II) was a tectonic quiescence phase in the SVC area and the low-rate sedimentation along the SVC area was rather constant, except in the current mouth of the canyon (Figs. 8, 9a, 10a). Here, the isochore

map reveals a small depocentre that may be related to the uplift of the HF or to the filling of an old rifting structure.

In the lower section of the SVC, the sedimentary record of Unit Id (Upper Oligocene to Middle Miocene) is eroded in the Tortonian due to the emplacement of the allochthonous HGU (Unit Ic). Therefore, the related isochore map (Fig. 9b) does not provide relevant information about the tectonic activity and sedimentation in this zone of the study area. However, the AR10 seismic profile (Fig. 8d) shows that the HGU is not present in the hanging wall of the HF at the intersection between the central and lower sections of the SVC. This evidence suggests that the lowermost section of the canyon is controlled by the HF and their activity started just before emplacement of the HGU. Thus, this is the oldest section of the SVC of Middle or Late Miocene age (Fig. 10b). The isochore map of Unit Id shows a small depocentre at the footwall of the current MPF and in the southern segment of the SVF (i.e., the upper section of the SVC) (Figs. 9a, b). According to the seismic data, these would correspond to the filling of pre-existing rifting structures (Fig. 8a, b).

MCS profiles show that within Unit Ib (Middle Miocene to Pliocene) there are various unconformities, onlapping reflectors, and thin chaotic units at the central and lower sections of the SVC (Fig. 8). In addition, the isochore map (Fig. 9c) reveals a clear depocenter located in the same area. These evidences suggest a contemporaneous sedimentation and progressive folding and uplift of the HF and MPF, which also generated accommodation space. This corresponds to the central segment of the canyon of Pliocene age (Fig. 10c). Unit Ib is locally eroded in the upper section (Fig. 9c), but there is no clear evidence that this unit has been eroded by the SVC at that time (Fig. 8a). The isochore map also shows a depocenter in the footwall of the northern segment of the MPF (Fig. 9c). The growth-strata configuration identified in the seismic data

(Fig. 8d) suggests synchronous sedimentation with the uplift of the fault. This tectonic activity would have generated accommodation space in the footwall block that may been filled by sediments coming from the surrounding morpho-structural highs (e.g., Marquês de Pombal and Gorringe Bank).

The Quaternary deposits are slightly folded both in the hanging-wall block of the MPF and in the upper and lower sections of the canyon. This evidence suggests that the Pliocene folding is currently active (Figs. 8a, 8c, 8d). This is not the case in the central section of the canyon, where seismic data shows the unfolded Plio-Quaternary Unit (Unit Ia) and no major tectonic structure can be identified (i.e., the lateral prolongation of the SVF or the HF) (Fig. 8b). The isochore map shows Unit Ia fully eroded along the canyon axis in the upper and central sections, and a highly diminished thickness in the lower section (Fig. 9d). The fairly rectilinear profile along the canyon axis (Fig. 4d) suggests that it has not yet reached its long-term equilibrium profile (e.g. Amblàs et al., 2011). Evidence for significant erosion is observed in the upper and central sections of the canyon (Fig. S1) most likely indicate that the canyon is trying to reach equilibrium. This observation provides further evidence about the relatively young age of the SVC. The isochore map shows three depocentres, one of them associated with the footwall block of the MPF (Fig. 9d). This observation may indicate that during this period the maximum activity or development of the MPF took place. Therefore, the incision of the SVC may have started at the Pliocene being maximum at the same time that the maximum development of the MPF (Fig.10d). Accordingly, this may suggest that the MPF plays an important role in the depositional dynamics of the canyon. All these observations indicate that the canyon likely developed in the late Quaternary from the central section, where erosion is largest and retrograded via mass movements on its flanks to its upper section and outer continental shelf (Figs. 10c, 10d). The incision

along the SVC axis makes the flanks unstable, which enhances retrogression and widening of the canyon (Baztan et al., 2005). Mass movements triggered by turbidity currents would have favoured the incision of the canyon and its progression towards the Horseshoe Abyssal Plain.

The isochore map of Unit Ia also shows two depocentres located on both sides of the SVC, at the Marquês de Pombal Block and the Sagres Plateau (Fig. 9d). These depocentres result from sediment contribution by geostrophic currents. This favours the sediment deposition on the head and flanks of the SVC (Hernández-Molina et al., 2003), which acts as a sediment trap for the MOW sediments.

Summarizing, the growth of the three faults (MPF, HF and SVF) has conditioned the entire existence of the canyon, from its orientation to its incision and width. The initial uplift of the HF generated a depocentre, which became an embryonic canyon with the subsequent evolution of the SVF and the MPF (Fig. 10). These structures are currently active, and their uplift conditions the incision and activity of the canyon (permanently in disequilibrium).

5.4. Local and global relevance of the São Vicente Canyon

Comparing the morphometric parameters (i.e., length, head depth, mouth depth, width, and S index and incision) of the SVC with the average in the global inventory of large submarine canyons (Harris and Whiteway, 2011) it turns out that , the SVC parameters are significantly larger (at least in terms of length and depth range) (Table S1, Fig. 11). A similar relationship can be found when comparing with the average of those parameters in submarine canyons of Western Europe (Table 1, Table S1, Fig. 11). According to the submarine canyon classification by Harris and Whiteway (2011), three different submarine canyons typologies can be distinguished: a) Type 1, shelf-incision with connection to a major river system; b) Type 2, shelf-incision without a connection

to a major river system; and c) Type 3, blind canyons. The SVC belongs to the Type 2 by definition, even though its morphometric parameters are closer to Type 1 (Fig. 11).

Table 1 shows the comparison between the morphometric parameters of different canyon systems of the West Iberian margin (i.e., Cascais, Setúbal and Lisbon canyons) with the canyons systems of the Southwest Iberian margin (i.e., São Vicente, Sagres, Lagos, Portimão and Faro canyons). The São Vicente, Setubal-Lisbon and Portimão canyons, the three being controlled by faults, have the longest straight length. Together with the Cascais Canyon, they have also the greatest depth range. In addition, their depth at the head is shallower and they all incise the continental shelf. In contrast, the Sagres and Faro canyons are shorter, less incised and their head is located on the slope. Among the compared canyons, the only canyon with a clear river connection, the Setubal-Lisboa Canyon belonging to type 1, is the wider canyon. However, the São Vicente and Portimão canyons also show morphometric parameters such as length, incision, head and mouth depth typical of submarine canyons fed by a large river, despite they have no clear connection to a fluvial system. Finally, when observing the trace of the MOW (Fig. 1), it is evident that the heads of submarine canyons of south and west Iberia coincide with the trace of the MOW, which may interact with other submarine canyons as it does with the SVC. The SVC has an important sedimentary contribution from the MOW current; therefore it could be classified as a new type of canyon, which is strongly influenced by bottom currents and also by active tectonic structures (faults). Despite some authors classify the Gulf of Cadiz as a passive margin (Harris and Whiteway, 2011), it has been demonstrated that it is an active margin that hosts the Present-day Eurasia-Africa plate boundary (e.g., Bartolome et al., 2012; Gràcia et al., 2003a, 2010;Martínez-Loriente et al., 2013, 2014, 2018; Sallarès et al., 2013; Terrinha et al., 2003; Zitellini et al., 2004, 2009).

Some of the world's largest submarine canyons that do not have a river connection are associated to active margins with subduction zones. In this context, the base level of these canyons is constantly changing. Therefore, the submarine canyons are not in equilibrium and are constantly incising and growing due to retrogressive erosion.

Some examples are the submarine canyons located on the Pacific plate subduction margin, such as the Bering canyon, 400 km-long (Harris and Whiteway, 2011); the Navarin canyon, 250 km-long (Carlson and Karl, 1988); the Zhemchug canyon, 196 km-long (Carlson and Karl, 1988); the Pribilof canyon, 145 km-long (Normark and Carlson, 2003); and the Monterey canyon, 111 km-long (Carlson and Karl, 1988); as well as submarine canyons associated to the subduction system of the Caribbean plate, such as the Great Bahama canyon, 175 km-long (Andrews et al., 1970). Thus, the SVC is a clear example of how a large submarine canyon may develop within an active and slow seismogenic margin.

6. Conclusions

A multiscale view of the SVC region using multibeam echo-sounder data, 2D multi-channel seismic profiles and sidescan sonar data allows us to carry out an accurate morpho-sedimentary and tectonic study of the processes occurring in the area. The SVC is the largest submarine canyon of the SW Iberian margin. The upper and the central sections of the SVC are deeply entrenched in the continental slope. The upper section shows a V-shape that progressively changes to a U-shape in the central section, whereas the lower section connects to the Horseshoe Abyssal Plain.

On the basis of its physiography and morphology, at present the SVC is not in equilibrium and shows erosive dynamics. In the upper and central sections of the canyon, retrogressive erosion and dismantling of the flanks predominate, indicating that

the canyon evolved from bottom-up. Submarine landslide deposits and landslide scars are the main processes that allowed bottom-up evolution of the canyon. The material resulting from the dismantling of the flanks and the MOW sedimentary deposits are the main sediment source, as the canyon is not fed by rivers. The MOW contributes material through two different processes: a) it deposits contourites on the flanks and head of the upper section of the canyon that periodically fail into the canyon; and b) the coarser-grained and denser sediment of the MOW might be trapped at the head of the canyon and could generates hyperpycnal flows. Erosion by these hyperpycnal and other sediment gravity flows forms steps at the canyon bed on its way to the mouth of the canyon. Most sediment gravity flows likely originate from destabilization of canyon flanks and contourites deposits by frequent seismic events in this area.

The origin of the canyon is fully tectonic. Initial uplift of the HF developed a synclinal fold at the base of the continental slope during an NNW-SSE trending compressive stage (late Miocene). This topographic relief, latter enhanced by evolution of the SVF and MPF, favoured the development of an embryonic canyon. During the Pliocene, the embryonic canyon developed towards the continental shelf by means of retrogressive mass-failures induced by the tectonic uplift and steep slope gradient. Full canyon development took place coinciding with the period of maximum activity of the MPF in the Quaternary. Therefore, the SVC is a diachronous and segmented canyon. Currently, the SVC shows a strong structural control and is conditioned by three main active faults (i.e., the MPF, the SVF and the HF).

7. Acknowledgements

The authors are grateful for funding from MINECO through projects HITS (AC 2011), IMPULS (REN 2003-05996/MAR), ESF-EUROCORES “EuroMargins” (REN2002-

11234-E MAR), SWIM (AE MCYT-DGI 2006), INSIGHT (CTM2015-70155-R), a MINECO FPI-2016 grant to Cristina S. Serra, and a MICINN "Juan de la Cierva-2017" grant to Sara Martínez-Loriente (ICM-CSIC). We thank Doug Masson, Russell Wynn, Chris Flewellen and the TOBI Team from the National Oceanography Centre (NOC, UK) for their assistance throughout the "HITS-2011" (PI E. Gràcia) data collection on board the RV "Hesperides". We are also indebted to Tim Le Bas (NOC, UK) for assisting O.G., J.G. and E.G. in processing the TOBI sidescan sonar data. MCS data were acquired during the RIFANO, BIGSETS and VOLTAIRE cruise (PI N. Zitellini). Grup Recerca Consolidat: 2017 SGR 1662.

8. References

Amblas, D., Gerber, T.P., Canals, M., Pratson, L.F., Urgeles, R., Lastras, G., Calafat, A.M., 2011. Transient erosion in the Valencia Trough turbidite systems, NW Mediterranean Basin. Geomorphology 130, 173–184. https://doi.org/10.1016/j.geomorph.2011.03.013

Amblas, D., Gerber, T.P., De Mol, B., Urgeles, R., Garcia-Castellanos, D., Canals, M., Pratson, L.F., Robb, M., Canning, J., 2012. Survival of a submarine canyon during long-term outbuilding of a continental margin. Geology 40, 543–546. https://doi.org/10.1130/G33178.1

Andrews, J., Shepard, F., Hurley, R., 1970. Great Bahama Canyon. Geol. Soc. Am. Bull. 81, 1061–1078.

Arzola, R.G., Wynn, R.B., Lastras, G., Masson, D.G., Weaver, P.P.E., 2008. Sedimentary features and processes in the Nazaré and Setúbal submarine canyons, west Iberian margin. Mar. Geol. 250, 64–88. https://doi.org/10.1016/j.margeo.2007.12.006

Baptista, M.A., Miranda, J.M., 2009. Revision of the portuguese catalog of tsunamis. Nat. Hazards Earth Syst. Sci. 9, 25–42. https://doi.org/10.5194/nhess-9-25-2009

Barkan, R., ten Brink, U.S., Lin, J., 2009. Far field tsunami simulations of the 1755 Lisbon earthquake: Implications for tsunami hazard to the U.S. East Coast and the Caribbean. Mar. Geol. 264, 109–122. https://doi.org/10.1016/j.margeo.2008.10.010

Bartolome, R., Gràcia, E., Stich, D., Martínez-Loriente, S., Klaeschen, D., de Lis Mancilla, F., Lo Iacono, C., Dañobeitia, J.J., Zitellini, N., 2012. Evidence for active strike-slip faulting along the Eurasia-Africa convergence zone: Implications for seismic hazard in the southwest Iberian margin. Geology 40, 495–498. https://doi.org/10.1130/G33107.1

Baztan, J., Berné, S., Olivet, J.L., Rabineau, M., Aslanian, D., Gaudin, M., Réhault, J.P., Canals, M., 2005. Axial incision : The key to understand submarine canyon evolution (in the western Gulf of Lion). Mar. Petrol. Geol. 22, 805-826 https://doi.org/10.1016/j.marpetgeo.2005.03.011

Blondel, P., Murton, B., 1997. Handbook of the seafloor sonar imagery. West Sussex, England.

Buforn, E., Sanz de Galdeano, C., Udías, A., 1995. Seismotectonics of the Ibero-Maghrebian region. Tectonophysics 248, 247–261. https://doi.org/10.1016/0040-1951(94)00276-F

Canals, M., Puig, P., De Madron, X.D., Heussner, S., Palanques, A., Fabres, J., 2006. Flushing submarine canyons. Nature 444, 354–357. https://doi.org/10.1038/nature05271

Carlson, P.R., Karl, H.A., 1988. Development of large submarine canyons in the Bering Sea, indicated by morphologic, seismic, and sedimentologic characteristics. Bull.

Geol. Soc. Am. 100, 1594–1615. https://doi.org/10.1130/0016-7606(1988)100<1594:DOLSCI>2.3.CO;2

Casalbore, D., Chiocci, F. L., Mugnozza, G. S., Tommasi, P., Sposato, A., 2011. Flash-flood hyperpycnal flows generating shallow-water landslides at Fiumara mouths in Western Messina Strait (Italy). Mar. Geophys. Res. 32(1-2), 257. https://doi.org/ 10.1007/s11001-011-9128-y

Casalbore, D., Bosman, A., Casas, D., Chiocci, F., Martorelli, E., Ridente, D., 2019. Morphological variability of submarine mass movements in the tectonically–Controlled calabro–Tyrrhenian continental margin (Southern Italy). Geosci. 9. https://doi.org/10.3390/geosciences9010043

Covault, J.A., Kostic, S., Paull, C.K., Sylvester, Z., Fildani, A., 2017. Cyclic steps and related supercritical bedforms: Building blocks of deep-water depositional systems, western North America. Mar. Geol. 393, 4–20. https://doi.org/10.1016/j.margeo.2016.12.009

Flewellen, C., Millard, N., Rouse, I., 1993. TOBI, a vehicle for deep ocean survey. Electron. Commun. Eng. J. 5, 85–93. https://doi.org/10.1049/ecej:19930015

Geissler, W.H., Matias, L., Stich, D., Carrilho, F., Jokat, W., Monna, S., Ibenbrahim, A., Mancilla, F., Gutscher, M.A., Sallars, V., Zitellini, N., 2010. Focal mechanisms for sub-crustal earthquakes in the Gulf of Cadiz from a dense OBS deployment. Geophys. Res. Lett. 37, 7–12. https://doi.org/10.1029/2010GL044289

Gràcia, E., Dañobeitia, J., Vergés, J., Bartolomé, R., Córdoba, D., 2003a. Crustal architecture and tectonic evolution of the Gulf of Cadiz (SW Iberian margin) at the convergence of the Eurasian and African plates. Tectonics 22, n/a-n/a. https://doi.org/10.1029/2001tc901045

Gràcia, E, Dañobeitia, J.J., Vergés, J., Team, P., 2003b. Mapping active faults offshore

Portugal (36°N-38°N): Implications for seismic hazard assessment in the SW Iberian Margin. Geology 31, 83–86. https://doi.org/10.1130/0091-7613(2003)031<0083

Gràcia, E., Pallàs, R., Soto, J.I., Comas, M., Moreno, X., Masana, E., Santanach, P., Diez, S., García, M., Dañobeitia, J., Bartolomé, R., Farrán, M., Gómez, M., Alpiste, M.J.R., Lastras, G., Wilmott, V., Perea, H., Blondel, P., Gómez, O., Bullock, L., Jacobs, C., Rouse, I., White, D., Whittle, S., Terrinha, P., Gafeira, J., Roque, C., 2006. Active faulting offshore SE Spain (Alboran Sea): Implications for earthquake hazard assessment in the Southern Iberian Margin. Earth Planet. Sci. Lett. 241, 734–749. https://doi.org/10.1016/j.epsl.2005.11.009

Gràcia, E., Vizcaino, A., Escutia, C., Asioli, A., Rodés, Á., Pallàs, R., Garcia-Orellana, J., Lebreiro, S., Goldfinger, C., 2010. Holocene earthquake record offshore Portugal (SW Iberia): testing turbidite paleoseismology in a slow-convergence margin. Quat. Sci. Rev. 29, 1156–1172. https://doi.org/10.1016/j.quascirev.2010.01.010

Grevemeyer, I., Lange, D., Villinger, H., Custódio, S., Matias, L., 2017. Seismotectonics of the Horseshoe Abyssal Plain and Gorringe Bank, eastern Atlantic Ocean. Constraints from ocean bottom seismometer data. J. Geophys. Res. Solid Earth 122, 63–78. https://doi.org/10.1002/2016JB013586

Harris, P.T., Whiteway, T., 2011. Global distribution of large submarine canyons: Geomorphic differences between active and passive continental margins. Mar. Geol. 285, 69–86. https://doi.org/10.1016/j.margeo.2011.05.008

Hayes, E., Pimm, A.C., Beckmann, P., Benson, W., Berger, W., Roth, P., Supko, P., 1972. Initial Reports of the Deep Sea Drilling Project. Government Printing Office, Washington D.C.

Hayward, N., Watts, A.B., Westbrook, J.K., Collier, J.S., 1999. A seismic reflection and GLORIA study of compressional deformation in the Gorringe Bank region, eastern North Atlantic, Geophys. J. Int., 138(3), 831–850. https://doi.org/10.1046/j.1365-246x.1999.00912.x

Hernández-Molina, F.J., Sierro, F.J., Llave, E., Roque, C., Stow, D.A.V., Williams, T., Lofi, J., Van der Schee, M., Arnáiz, A., Ledesma, S., Rosales, C., Rodríguez-Tovar, F.J., Pardo-Igúzquiza, E., Brackenridge, R.E., 2015. Evolution of the gulf of Cadiz margin and southwest Portugal contourite depositional system: Tectonic, sedimentary and paleoceanographic implications from IODP expedition 339. Mar. Geol. 377, 7–39. https://doi.org/10.1016/j.margeo.2015.09.013

Hernández-Molina, J., Stow, D., Alvarez-Zarikian, C., Expedition IODP 339 Scientists., 2013. IODP Expedition 339 in the Gulf of Cadiz and off West Iberia: decoding the environmental significance of the Mediterranean outflow water and its global influence. Sci. Dril., 16, 1–11. https://doi.org/10.5194/sd-16-1-2013

Hernández-Molina, J., Llave, E., Somoza, L., Fernández-Puga, M.C., Maestro, A., León, R., Medialdea, T., Barnolas, A., García, M., Díaz del Río, V., Fernández-Salas, L.M., Vázquez, J.T., Lobo, F., Alveirinho Dias, J.M., Rodero, J., Gardner, J., 2003. Looking for clues to paleoceanographic imprints: A diagnosis of the Gulf of Cadiz contourite depositional systems. Geology 31, 19–22. https://doi.org/10.1130/0091-7613(2003)031<0019:LFCTPI>2.0.CO;2

Hughes Clarke, J., 2016. First wide-angle view of channelized turbidity currents links migrating cyclic steps to flow characteristics. *Nat Commun* 7, 11896. https://doi.org/10.1038/ncomms11896

Iribarren, L., Vergés, J., Camurri, F., Fullea, J., Fernàndez, M., 2007. The structure of the Atlantic-Mediterranean transition zone from the Alboran Sea to the Horseshoe

Abyssal Plain (Iberia-Africa plate boundary). Mar. Geol. 243, 97–119. https://doi.org/10.1016/j.margeo.2007.05.011

Lastras, G., Arzola, R.G., Masson, D.G., Wynn, R.B., Huvenne, V.A.I., Hühnerbach, V., Canals, M., 2009. Geomorphology and sedimentary features in the Central Portuguese submarine canyons, Western Iberian margin. Geomorphology 103, 310–329. https://doi.org/10.1016/j.geomorph.2008.06.013

Llave, E., Matias, H., Hernández-Molina, F.J., Ercilla, G., Dorrik A., Stow, V., Medialdea, T., 2011. Pliocene–Quaternary contourites along the northern Gulf of Cadiz margin: sedimentary stacking pattern and regional distribution. Geo-Mar Lett 31, 377–390. https://doi.org/ 10.1007/s00367-011-0241-3

Leopold, L., Wolman, M., 1957. River channel patterns - braided, meandring and stright. United States Geol. Surv. Prof. Pap. 282-B.

Lewis, K.B., Barnes, P.M., 1999. Kaikoura Canyon, New Zealand: Active conduit from near-shore sediment zones to trench-axis channel. Mar. Geol. 162, 39–69. https://doi.org/10.1016/S0025-3227(99)00075-4

Lozano, L., Cantavella, J.J., Barco, J., 2019. A new 3-D P-wave velocity model for the Gulf of Cadiz and adjacent areas derived from controlled-source seismic data: application to non-linear probabilistic relocation of moderate earthquakes. Geophys. J. Int. ggz562, 1–57. https://doi.org/10.1093/gji/ggz562

Marchès, E., Mulder, T., Cremer, M., Bonnel, C., Hanquiez, V., Gonthier, E., Lecroart, P., 2007. Contourite drift construction influenced by capture of Mediterranean Outflow Water deep-sea current by the Portimão submarine canyon (Gulf of Cadiz, South Portugal). Mar. Geol. 242, 247–260. https://doi.org/10.1016/j.margeo.2007.03.013

Martínez-Loriente, S., Gràcia, E., Bartolome, R., Perea, H., Klaeschen, D., Dañobeitia,

J.J., Zitellini, N., Wynn, R.B., Masson, D.G., 2018. Morphostructure, tectono-sedimentary evolution and seismic potential of the Horseshoe Fault, SW Iberian Margin. Basin Res. 30, 382–400. https://doi.org/10.1111/bre.12225

Martínez-Loriente, S., Gràcia, E., Bartolome, R., Sallarès, V., Connors, C., Perea, H., Lo Iacono, C., Klaeschen, D., Terrinha, P., Dañobeitia, J.J., Zitellini, N., 2013. Active deformation in old oceanic lithosphere and significance for earthquake hazard: Seismic imaging of the Coral Patch Ridge area and neighboring abyssal plains (SW Iberian Margin). Geochemistry, Geophys. Geosystems 14, 2206–2231. https://doi.org/10.1002/ggge.20173

Martínez-Loriente, S., Sallarès, V., Gràcia, E., Bartolome, R., Dañobeitia, J.J., Zitellini, N., 2014. Seismic and gravity constraints on the nature of the basement in the Africa-Eurasia plate boundary: New insights for the geodynamic evolution of the SW Iberian margin. J. Geophys. Res. Solid Earth 119, 127–149. https://doi.org/10.1002/2013JB010476

Masson, D.G., Wynn, R.B., Bett, B., 2004. Sedimentary environment of the Faroe-Shetland and Faroe Bank Channels, north-east Atlantic, and the use of bedforms as indicators of bottom current velocity in the deep ocean. Sedimentology 51, 1207–1241. https://doi.org/10.1111/j.1365-3091.2004.00668.x

Mastbergen, D.R., Van Den Berg, J.H., 2003. Breaching in fine sands and the generation of sustained turbidity currents in submarine canyons. Sedimentology 50, 625–637. https://doi.org/10.1046/j.1365-3091.2003.00554.x

Mauffrey, M.A., Urgeles, R., Berné, S., Canning, J., 2017. Development of submarine canyons after the Mid-Pleistocene Transition on the Ebro margin, NW Mediterranean: The role of fluvial connections. Quat. Sci. Rev. 158, 77–93. https://doi.org/10.1016/j.quascirev.2017.01.006

Medialdea, T., Vegas, R., Somoza, L., Vázquez, J.T., Maldonado, A., Díaz-del-Río, V., Maestro, A., Córdoba, D., Fernández-Puga, M.C., 2004. Structure and evolution of the "Olistostrome" complex of the Gibraltar Arc in the Gulf of Cadiz (eastern Central Atlantic): Evidence from two long seismic cross-sections, Mar. Geol., 209(1–4), 173–198. https://doi.org/10.1016/j.margeo.2004.05.029

Micallef, A., Mountjoy, J.J., Barnes, P.M., Canals, M., Lastras, G., 2014. Geomorphic response of submarine canyons to tectonic activity: Insights from the Cook Strait canyon system, New Zealand. Geosphere 10, 905–929 https://doi.org/10.1130/GES01040.1

Mulder, T., Lecroart, P., Hanquiez, V., Marches, E. Gonthier, E., Guedes, J.C., Thiébot, E., Jaaidi, B., Kenyon, N., Voisset, M., Perez, C., Sayago, M., Fuchey, Y., Bujan, S., 2006. The western part of the Gulf of Cadiz: Contour currents and turbidity currents interactions. Geo-Marine Lett. 26, 31–41. https://doi.org/10.1007/s00367-005-0013-z

Mulder, T., Syvitski, J.P.M., Migeon, S., Faugères, J.C., Savoye, B., 2003. Marine hyperpycnal flows: Initiation, behaviorand related deposits. A review. Mar. Pet. Geol. 20, 861–882 https://doi.org/10.1016/j.marpetgeo.2003.01.003

Neres, M., Carafa, M.M.C., Fernandes, R.M.S., Matias, L., Duarte, J.C., Barba, S., Terrinha, P., 2016. Lithospheric deformation in the Africa-Iberia plate boundary: Improved neotectonic modeling testing a basal-driven Alboran plate. J. Geophys. Res. Solid Earth 121, 6566–6596. https://doi.org/10.1002/2016JB013012

Nocquet, J.M., Calais, E., 2004. Geodetic measurements of crustal deformation in the Western Mediterranean and Europe. Pure Appl. Geophys. 161, 661–681. https://doi.org/10.1007/s00024-003-2468-z

Normark, W.R., Carlson, P.R., 2003. Giant submarine canyons: Is size any clue to their

importance in the rock record? Spec. Pap. Geol. Soc. Am. 370, 175–190. https://doi.org/10.1130/0-8137-2370-1.175

Oliveira, A., Santos, A.I., Rodrigues, A., Vitorino, J., 2007. Sedimentary particle distribution and dynamics on the Nazaré canyon system and adjacent shelf (Portugal). Mar. Geol. 246, 105–122. https://doi.org/10.1016/j.margeo.2007.04.017

Palanques, A., Durrieu de Madron, X., Puig, P., Fabres, J., Guillén, J., Calafat, A., Canals, M., Heussner, S., Bonnin, J., 2006. Suspended sediment fluxes and transport processes in the Gulf of Lions submarine canyons. The role of storms and dense water cascading. Mar. Geol. 234, 43–61. https://doi.org/10.1016/j.margeo.2006.09.002

Pereira, R., Alves, T.M., 2013. Crustal deformation and submarine canyon incision in a Meso-Cenozoic first-order transfer zone (SW Iberia, North Atlantic Ocean). Tectonophysics 601, 148–162. https://doi.org/10.1016/j.tecto.2013.05.007

Pierdomenico, M., Casalbore, D., Chiocci, F. L., 2019. Massive benthic litter funnelled to deep sea by flash-flood generated hyperpycnal flows. *Sci Rep* 9**,** 5330. https://doi.org/10.1038/s41598-019-41816-8

Piper, D.J.W., Normark , William R., 2009. Processes That Initiate Turbidity Currents and Their Influence on Turbidites: A Marine Geology Perspective Title. J. Sediment. Res. 79, 347–362.

Puig, P., Palanques, A., Martín, J., 2014. Contemporary Sediment-Transport Processes in Submarine Canyons. Ann. Rev. Mar. Sci. 6, 53–77. https://doi.org/10.1146/annurev-marine-010213-135037

Sallarès, V., Gailler, A., Gutscher, M.A., Graindorge, D., Bartolomé, R., Gràcia, E., Díaz, J., Dañobeitia, J.J., Zitellini, N., 2011. Seismic evidence for the presence of Jurassic oceanic crust in the central Gulf of Cadiz (SW Iberian margin). Earth

Planet. Sci. Lett. 311, 112–123. https://doi.org/10.1016/j.epsl.2011.09.003

Sallarès, V., Martínez-Loriente, S., Prada, M., Gràcia, E., Ranero, C., Gutscher, M.A., Bartolome, R., Gailler, A., Dañobeitia, J.J., Zitellini, N., 2013. Seismic evidence of exhumed mantle rock basement at the Gorringe Bank and the adjacent Horseshoe and Tagus abyssal plains (SW Iberia). Earth Planet. Sci. Lett. 365, 120–131. https://doi.org/10.1016/j.epsl.2013.01.021

Schettino, A., Turco, E., 2009. Breakup of Pangaea and plate kinematics of the central Atlantic and Atlas regions. Geophys. J. Int. 178, 1078–1097. https://doi.org/10.1111/j.1365-246X.2009.04186.x

Serra, N., Ambar, I., Käse, R.H., 2005. Observations and numerical modelling of the Mediterranean outflow splitting and eddy generation. Deep-Sea Research II. 52, 383–408. https://doi.org/ 10.1016/j.dsr2.2004.05.025

Shepard, F.P., 1981. Submarine canyons_multiple causes and long-time persistence. Pet. Geol. Bull 65, 1062–1077.

Silva, S., Terrinha, P., Matias, L., Duarte, J.C., Roque, C., Ranero, C.R., Geissler, W.H., Zitellini, N., 2017. Micro-seismicity in the Gulf of Cadiz: Is there a link between micro-seismicity, high magnitude earthquakes and active faults? Tectonophysics 717, 226–241. https://doi.org/10.1016/j.tecto.2017.07.026

Stich, D., Mancilla, F. de L., Morales, J., 2005. Crust-mantle coupling in the Gulf of Cadiz (SW-Iberia). Geophys. Res. Lett. 32, 1–4. https://doi.org/10.1029/2005GL023098

Stich, D., Serepelloni, E., Mancilla, F., Morales, J., 2006. Kinematics of the Iberia–Maghreb plate contact from seismic moment tensors and GPS observations. Tectonophysics 426, 295–317. https://doi.org/10.1016/j.tecto.2006.08.004

Terrinha, P., Duarte, H., Brito, P., Noiva, J., Ribeiro, C., Omira, R., Baptista, M.A.,

Miranda, M., Magalhães, V., Roque, C., 2019. The Tagus River delta landslide, off Lisbon, Portugal. Implications for Marine geo-hazards. Mar. Geol. 416, 105983. https://doi.org/10.1016/j.margeo.2019.105983

Terrinha, P., Matias, L., Vicente, J., Duarte, J., Luís, J., Pinheiro, L., Lourenço, N., Diez, S., Rosas, F., Magalhães, V., Valadares, V., Zitellini, N., Roque, C., Víctor, L.M., 2009. Morphotectonics and strain partitioning at the Iberia-Africa plate boundary from multibeam and seismic reflection data. Mar. Geol. 267, 156–174. https://doi.org/10.1016/j.margeo.2009.09.012

Terrinha, P., Pinheiro, L.M., Henriet, J.P., Matias, L., Ivanov, M.K., Monteiro, J.H., Akhmetzhanov, A., Volkonskaya, A., Cunha, T., Shaskin, P., Rovere, M., 2003. Tsunamigenic-seismogenic structures, neotectonics, sedimentary processes and slope instability on the southwest Portuguese Margin. Mar. Geol. 195, 55–73. https://doi.org/10.1016/S0025-3227(02)00682-5

Torelli, L., Sartori, R., Zitellini, N., 1997. The giant chaotic body in the Atlantic Ocean off Gibraltar: New results from a deep seismic reflection survey. Mar. Pet. Geol. 14, 125–134. https://doi.org/10.1016/S0264-8172(96)00060-8

Tortella, D., Torne, M., Perez-Estaun, A., 1997. Geodynamic evolution of the eastern segment of the Azores–Gibraltar Zone: The Gorringe Bank and Gulf of Cadiz region, Mar. Geophys. Res., 19, 211–230.Vizcaino, A., Gràcia, E., Pallàs, R., Terrinha, P., Diez, S., Dañobeitia, J., D, M., 2005. Active tectonic and sedimentary processes along the Sao Vicente Canyon (SW Iberian Margin): High-Resolution Imaging. Eur. Geosci. Union 2005 7, 7707.

Zitellini, N., Chierici, F., Sartori, R., Torelli, L., 1999. The tectonic source of the 1755 Lisbon earthquake and tsunami. Ann. di Geofis. 42, 49–55. https://doi.org/10.4401/ag-3699

Zitellini, N., Gràcia, E., Matias, L., Terrinha, P., Abreu, M.A., De Alteriis, G., Henriet, J.P., Dañobeitia, J.J., Masson, D.G., Mulder, T., Ramella, R., Somoza, L., Diez, S., 2009. The quest for the Africa-Eurasia plate boundary west of the Strait of Gibraltar. Earth Planet. Sci. Lett. 280, 13–50. https://doi.org/10.1016/j.epsl.2008.12.005

Zitellini, N., Mendes, L.A., Cordoba, D., Danobeitia, J., Nicolich, R., Pellis, G., Ribeiro, A., Sartori, R., Torelli, L., Bartolome, R., Bortoluzzi, G., Calafato, A., Carrilho, F., Casoni, L., Chierici, E., Corela, C., Correggiari, A., Delia Vedova, B., Gracia, E., Jornet, P., Landuzzi, M., Ligi, M., Magagnoli, A., Marozzi, G., Matias, L., Penitenti, D., Rodriguez, P., Rovere, M., Terrinha, P., Vigliotti, L., Ruiz, A.Z., 2001. Source of 1755 lisbon earthquake and tsunami investigated. Eos (Washington. DC). 82, 285–291. https://doi.org/10.1029/EO082i026p00285-01

Zitellini, N., Rovere, M., Terrinha, P., Chierici, F., Matias, L., Victor, L.M., Corela, C., Ribeiro, A., Cordoba, D., Danobeitia, J.J., Grácia, E., Bartolomé, R., Nicolich, R., Pellis, G., Della Vedova, B., Sartori, R., Torelli, L., Correggiari, A., Vigliotii, L., 2004. Neogene through quaternary tectonic reactivation of SW Iberian passive margin. Pure Appl. Geophys. 161, 565–587. https://doi.org/10.1007/s00024-003-2463-4

Figure 1. Bathymetric map of the Gulf of Cadiz with the location of the main faults (after Martínez-Loriente et al., 2013, 2018). Yellow circles correspond to epicenter locations for the period 1400–2020 (Instituto Geográfico Nacional [IGN] catalogue; http://www.ign.es/ign/layout/sismo.do. Earthquakes locations according to Lozano et al., 2019 and Stich et al., 2006. Inset: Plate tectonic setting of the SW Iberian margin at the boundary between the Eurasian and African Plates. The grey rectangle corresponds

to the area depicted in Figure 1. Cc: Cascais canyon; CPR: Coral Patch Ridge; CPRF: Coral Patch Ridge Fault; CPS: Coral Patch Seamount; CSV: Cape São Vicente; Fc: Faro canyon; GB: Gorringe Bank; GBF: Gorringe Bank Fault; GCIW: Gulf of Cadiz Imbricated Wedge; HF: Horseshoe Fault; IDHB: Infante Don Henrique Basin; Lc: Lagos canyon; LN: Lineament North; LS: Lineament South; MPF: Marquês de Pombal Fault; MPFB: Marquês de Pombal Fault Block; PBF: Portimão Bank Fault; Pc: Portimão canyon; PSF: Pereira de Sousa Fault; SAc: Sagres canyon; Sc: Setúbal canyon; SH: Seine Hills; SP: Sagres Plateau; SVC: São Vicente Canyon; SVF: São Vicente Fault.

Figure 2. Bathymetric map of the study area in the SW Portuguese Margin. The grey area depicts the TOBI sidescan sonar mosaic of the São Vicente Canyon (SVC) acquired during the HITS-2001 survey (Gràcia et al., 2003a). White lines label the multichannel seismic (MCS) profiles used in this study and acquired during the BIGSETS-1998 (BS), ARRIFANO-1992 (AR) and VOLTAIRE-2004 (VOL) surveys (e.g. Zitellini et al., 2001, 2004; Terrinha et al., 2003). Thick white lines represent the seismic sections shown in Figure 8.

Figure 3. Slope maps superimposed on the 3D bathymetry of the São Vicente Canyon (SVC). The slope is represented as percentages in dark blue for the lowest slope (0%) and red for the highest slope (≥ 50%). a), b) and c) correspond to the Upper, Central and Lower sections of the canyon. HFB: Horseshoe Fault Basin.

Figure 4. Northwest-southeast oriented bathymetric profiles across the São Vicente Canyon at the Upper, Central, and Lower sections (a, b, and c, respectively); and d) Bathymetric longitudinal profile along the São Vicente Canyon axis.

Figure 5. a) TOBI sidescan sonar image of the Upper section of the São Vicente Canyon. b) Interpreted TOBI mosaic of the same area identifying flow structures, tectonic structures, slope structures, and sedimentary features.

Figure 6. a) TOBI sidescan sonar image of the Central section of São Vicente Canyon. b) Interpreted TOBI mosaic of the same area labelling the main features of the area. See legend in Fig. 5.

Figure 7. a) TOBI sidescan sonar image of the Lower section of São Vicente Canyon. b) Interpreted TOBI mosaic of the same area identifying the main elements of this sector. See legend in Fig. 5 (modified from Martínez-Loriente et al., 2018).

Figure 8. Interpreted sections of 4 multichannel seismic profiles in time across the three sections of the São Vicente Canyon. See location in Figure 2. Stratigraphy from Martínez-Loriente et al., 2013 (see Figure S2). Ia= Plio-Quaternary; Ib= Middle Miocene - Pliocene; Ic-HGU= Horseshoe gravitational unit; Id= Upper Pligocene - Middle Miocene; II= Upper Cretaceous - Lower Eocene; III= Cretaceous; IV= Lower Cretaceous; V= Upper Jurassic; VI= Basement; HF: Horseshoe Fault; MPF: Marquês de Pombal Fault; MPB: Marquês de Pombal Block; IDHB: Infante Don Henrique Basin; SP: Sagres Plateau; SVF: São Vicente Fault; SVC: São Vicente Canyon; TWTT: Two-way travel time. VE (vertical exaggeration) = 2.

Figure 9. Isochore maps that illustrate the variation in thicknesses of the different stratigraphic units over time: a) Upper Cretaceous – Early Eocene (Unit II); b) Upper Oligocene – Middle Miocene (Unit Id); c) Middle Miocene – Pliocene (Unit Ib); and d) Plio-Quaternary (Unit Ia). HF: Horseshoe Fault; MOW: Mediterranean Outflow Water; MPF: Marquês de Pombal Fault; SVC: São Vicente Canyon; SVF: São Vicente Fault; TWTT: Two-way travel time, in seconds.

Figure 10. Formation and evolution model of the São Vicente area from the Upper Cretaceous to the Plio-Quaternary, including the São Vicente Fault (SVF), the Horseshoe Fault (HF) and Marquês de Pombal Fault (MPF). D: Depocentre; M.M.-P.: Middle Miocene-Pliocene; P-Q: Plio-Quaternary; U.C.-E.E.: Upper Cretaceous-Early Eocene; U.O.-M.M.: Upper Oligocene-Middle Miocene; SVC: São Vicente Canyon.

Figure 11. Plot of the mean statistics of the submarine canyons in order of length (km), slope (º), sinuosity (º), and depth range (km). Classification of canyons according to Harris et al. (2011). Morphometric parameter averages (see in supplementary material Table S1) of the submarine canyons in Western Europe and global average of canyon types from Harris and Whiteway, (2011).

Table 1. Characterization of the largest west and southwest Iberian canyons in comparison to the São Vicente Canyon

Declaration of interests

☒ The authors declare that they have no known competing financial interests or personal relationships that could have appeared to influence the work reported in this paper.

☐The authors declare the following financial interests/personal relationships which may be considered as potential competing interests:

Table 1. Morphometric parameters of the canyons in the west and southwest Iberian margin.

Canyon	*Straight length (km)*	*Depth at the head (mbsl)*	*Mouth depth (mbsl)*	*Width (km)*	*S Index*	*Tectonic control*	*Max. Incision (m)*	*River connection*	*Information Source*	*Canyon type* [(1)]
Cascais	61.5	175	4600	4.2-28	1.44	Unknown	1800	No	Lastras et al., 2009	Type 2
Setúbal-Lisbon	145.8	150	4800	7.8-40	1.2	Lower Tagus fault zone and Grãndola fault	2200	Tagus and Sado rivers	Lastras et al., 2009	Type 1
São Vicente	**157**	**200**	**4900**	**1.5-3.5**	**1.12**	**MPF, SVF, HF**	**2000**	**No**	**This study**	**Type 2**
Sagres	41.7	1300	4200	1.26-2.89	1.06	Unknown	300	No	This study	Type 3
Lagos	56	760	3600	2.46-12.4	1.16	Unknown	1500	No	(Marchès et al., 2007) & this study	Type 3
Portimão	134.7	100	4000	2.3-5.7	1.15	Portimão Fault	1600	Unknow	(Marchès et al., 2007) & this study	Type 2
Faro	48	1300	2700	4.9-11.8	1.16	Unknown	700	No	This study	Type 3

(1) According to the classification by Harris and Whiteway (2011).

- Largest submarine canyons may not be associated to river systems.
- Canyons can be generated by folding during a compressive stage.
- Young canyons are conditioned by active fault systems.
- Flank erosion and bottom currents are the sediment sources of canyons without a river connection.
- Submarine landslides are the main source of retrogressive erosion.

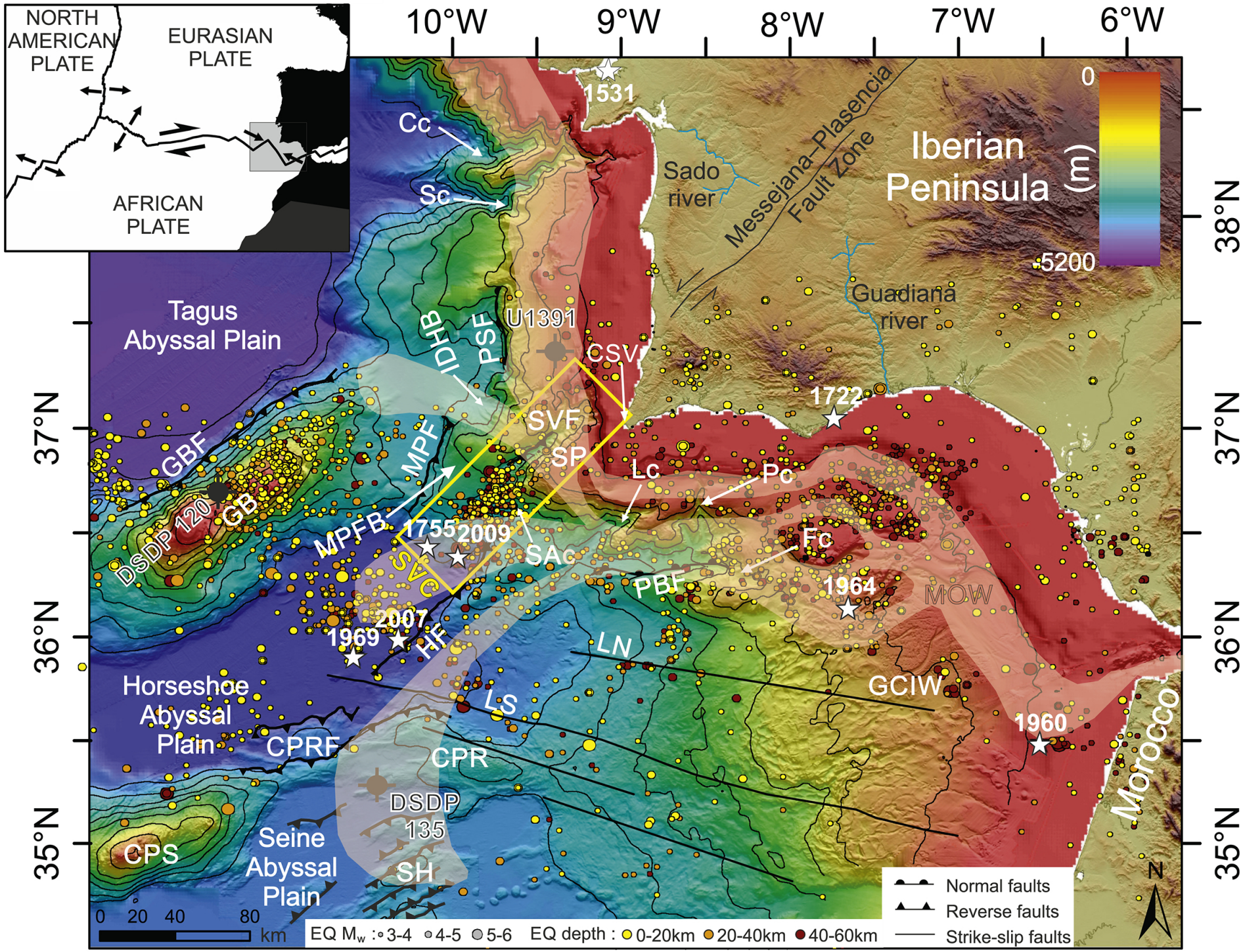
NORTH AMERICAN PLATE
EURASIAN PLATE
AFRICAN PLATE
10°W
9°W
8°W
7°W
6°W
38°N
37°N
36°N
35°N
1531
Cc
Sc
Sado river
Messejana–Plasencia Fault Zone
Iberian Peninsula
0
(m)
5200
Guadiana river
Tagus Abyssal Plain
IDHB
PSF
U1391
CSV
SVF
SP
1722
GBF
MPF
MPFB
GB
DSDP 120
1755
2009
SAc
SVc
Lc
Pc
Fc
PBF
MOW
1964
2007
1969
HF
LN
LS
GCIW
1960
Morocco
Horseshoe Abyssal Plain
CPRF
CPR
DSDP 135
SH
CPS
Seine Abyssal Plain
0 20 40 80
km
EQ Mw : 3-4 4-5 5-6
EQ depth : 0-20km 20-40km 40-60km
Normal faults
Reverse faults
Strike-slip faults
N

Figure 1

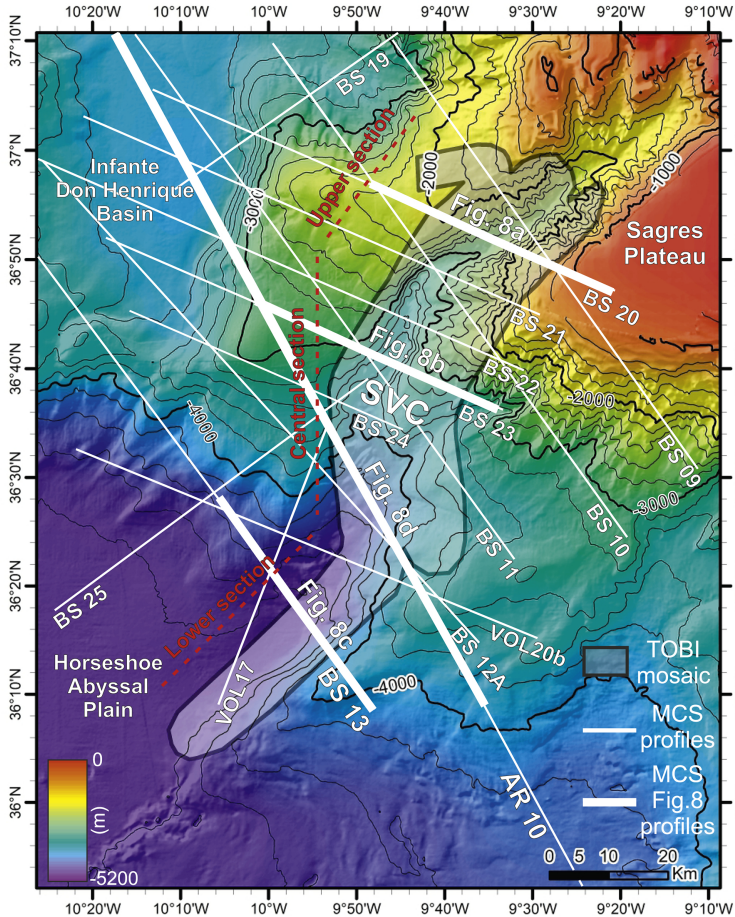
10°20'W
10°10'W
10°W
9°50'W
9°40'W
9°30'W
9°20'W
9°10'W
37°10'N
37°N
36°50'N
36°40'N
36°30'N
36°20'N
36°10'N
36°N
Infante
Don Henrique
Basin
Horseshoe
Abyssal
Plain
Sagres
Plateau
SVC
Upper section
Central section
Lower section
BS 19
BS 20
BS 21
BS 22
BS 23
BS 24
BS 09
BS 10
BS 11
BS 12A
BS 13
BS 25
VOL17
VOL20b
Fig. 8a
Fig. 8b
Fig. 8c
Fig. 8d
-1000
-2000
-3000
-4000
0
(m)
-5200
TOBI
mosaic
MCS
profiles
MCS
Fig.8
profiles
AR 10
0 5 10 20
Km

Figure 2

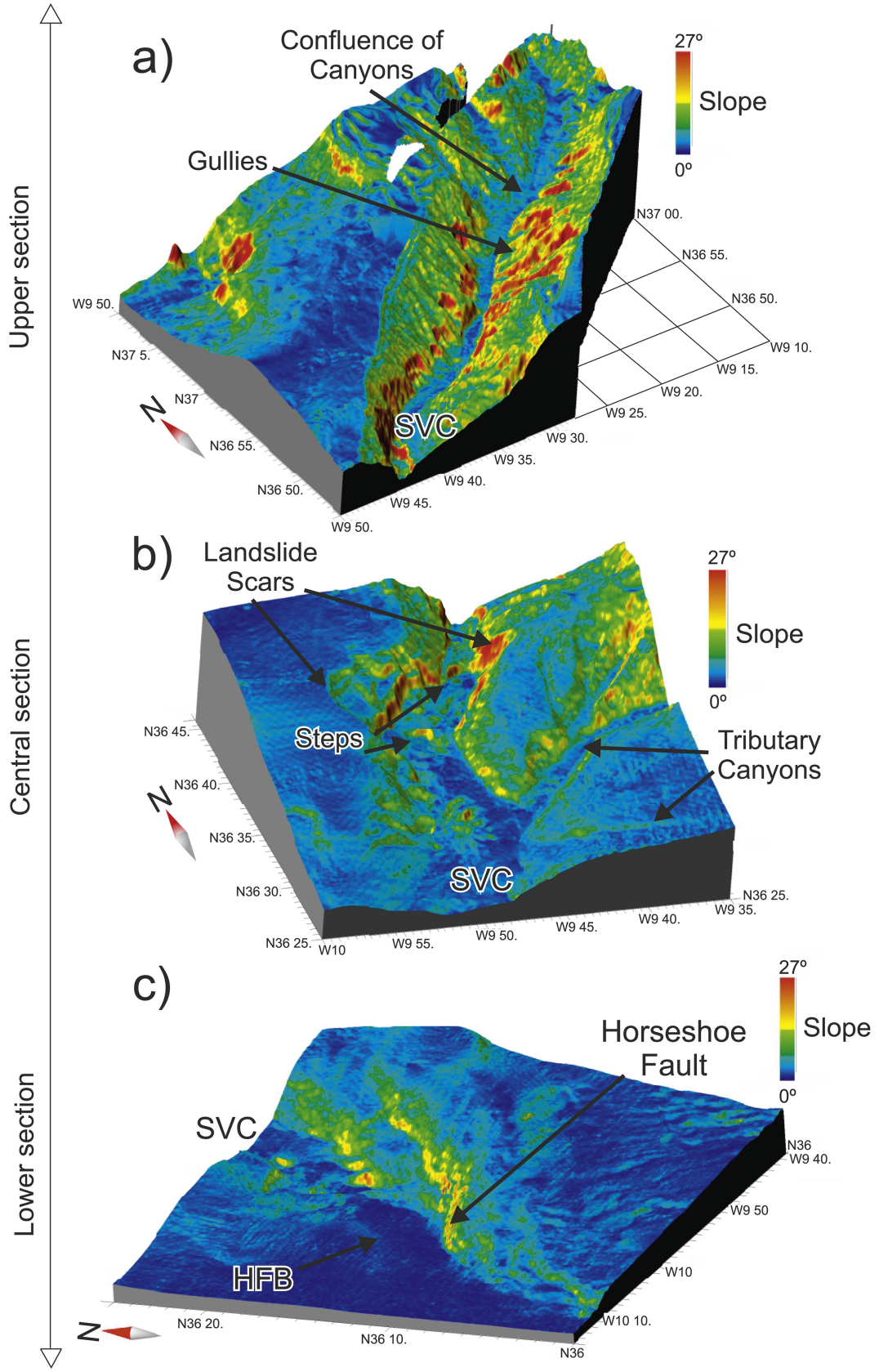
Upper section
Central section
Lower section
a)
Confluence of Canyons
Gullies
27°
Slope
0°
SVC
N37 00.
N36 55.
N36 50.
W9 10.
W9 15.
W9 20.
W9 25.
W9 30.
W9 35.
W9 40.
W9 45.
W9 50.
W9 50.
N37 5.
N37
N36 55.
N36 50.
N
b)
Landslide Scars
Steps
Tributary Canyons
SVC
N36 45.
N36 40.
N36 35.
N36 30.
N36 25.
W10
W9 55.
W9 50.
W9 45.
W9 40.
W9 35.
N36 25.
c)
Horseshoe Fault
SVC
HFB
N36 20.
N36 10.
N36
W10 10.
W10
W9 50
N36
W9 40.

Figure 3

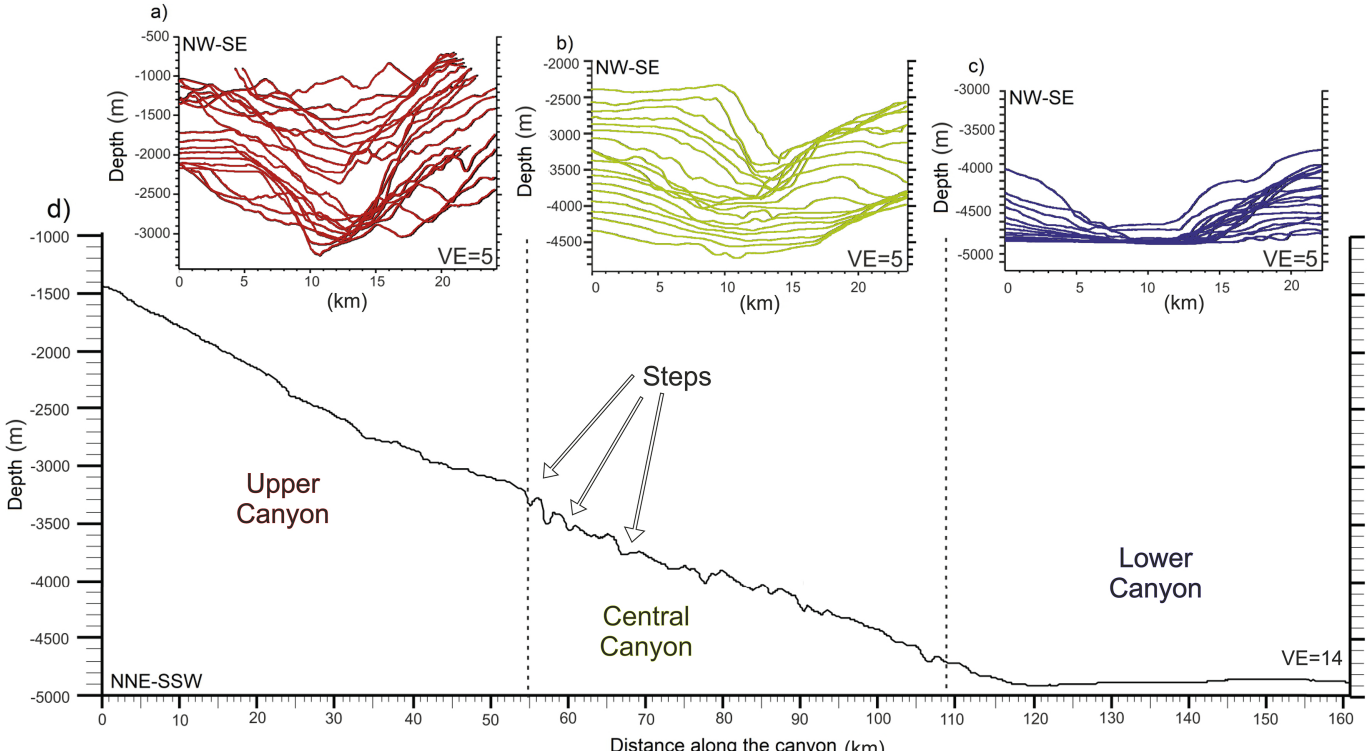
a)
NW-SE
Depth (m)
VE=5
(km)
b)
NW-SE
Depth (m)
VE=5
(km)
c)
NW-SE
Depth (m)
VE=5
(km)
d)
Depth (m)
Steps
Upper Canyon
Central Canyon
Lower Canyon
NNE-SSW
VE=14
Distance along the canyon (km)

Figure 4

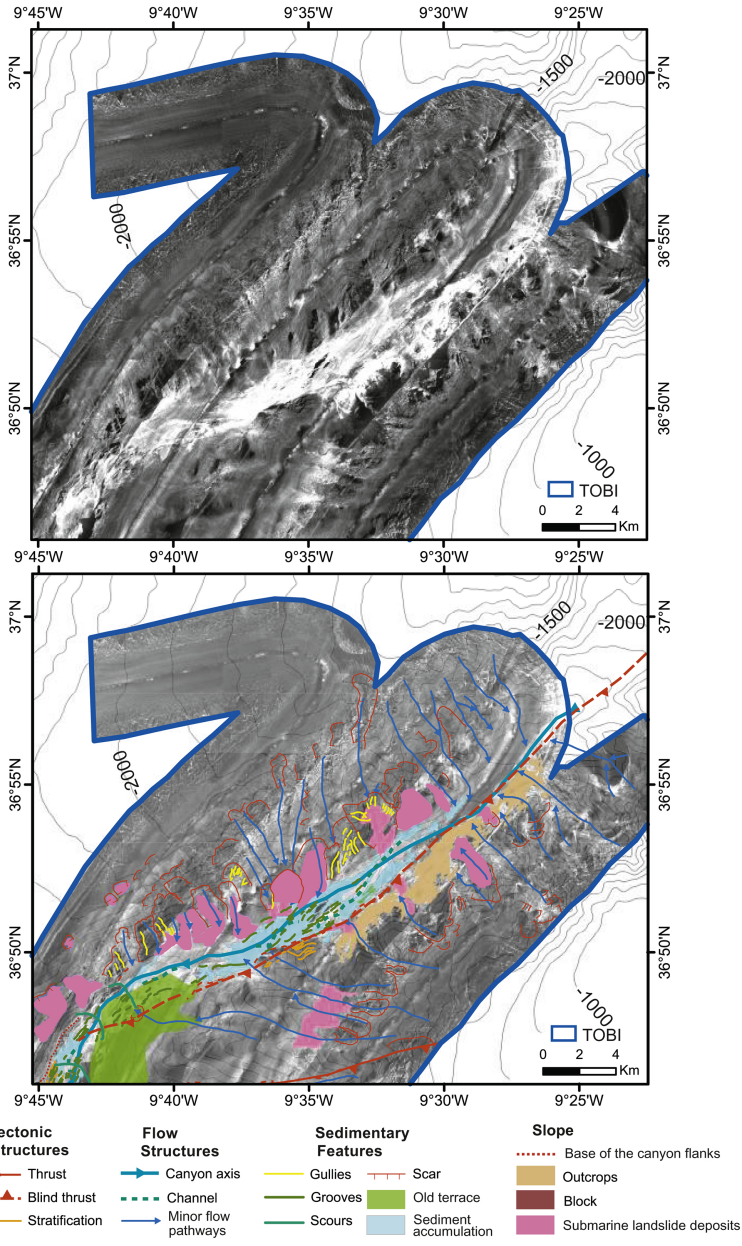
9°45'W
9°40'W
9°35'W
9°30'W
9°25'W
37°N
36°55'N
36°50'N
-1500
-2000
-1000
TOBI
0 2 4
Km
Tectonic Structures
Thrust
Blind thrust
Stratification
Flow Structures
Canyon axis
Channel
Minor flow pathways
Sedimentary Features
Gullies
Grooves
Scours
Scar
Old terrace
Sediment accumulation
Slope
Base of the canyon flanks
Outcrops
Block
Submarine landslide deposits

Figure 5

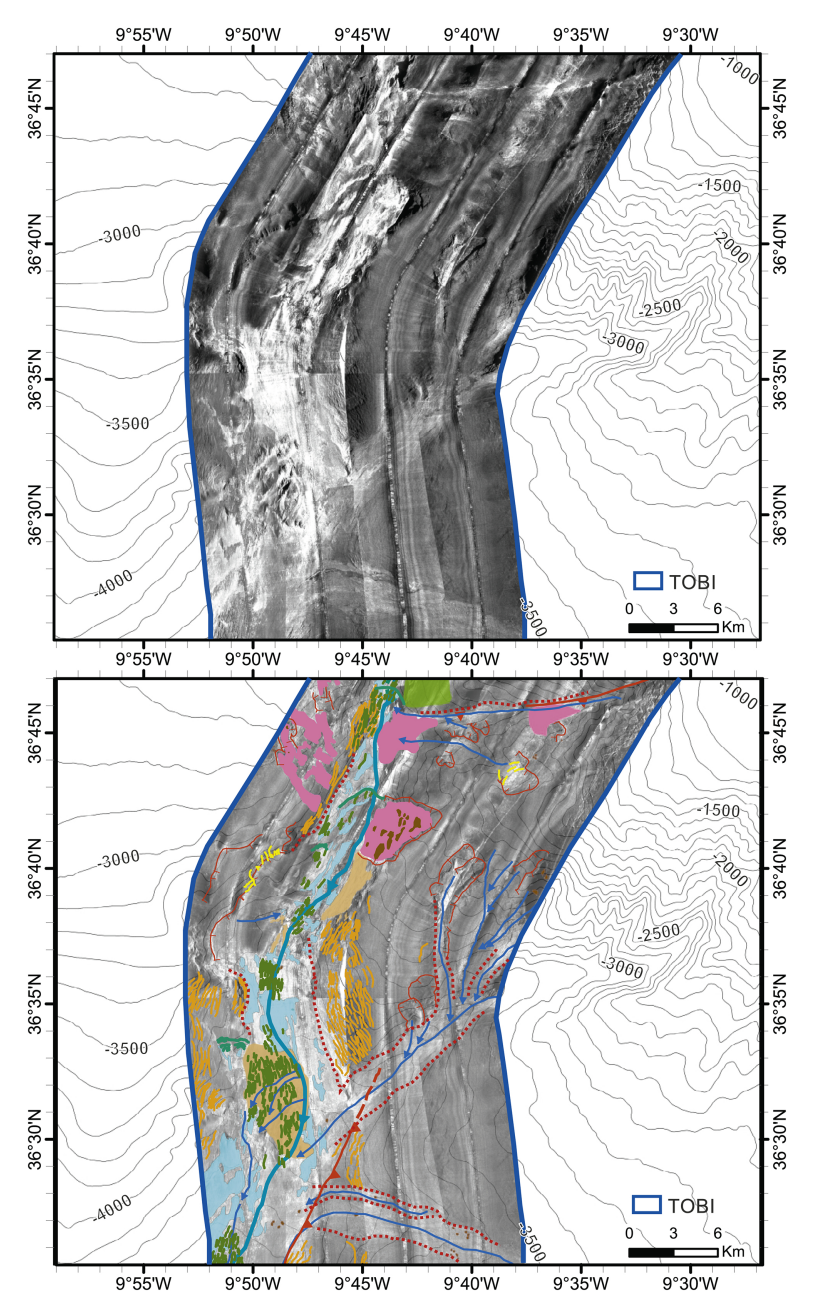
9°55'W
9°50'W
9°45'W
9°40'W
9°35'W
9°30'W
36°45'N
36°40'N
36°35'N
36°30'N
-1000
-1500
-2000
-2500
-3000
-3500
-4000
TOBI
0 3 6
Km

Figure 6

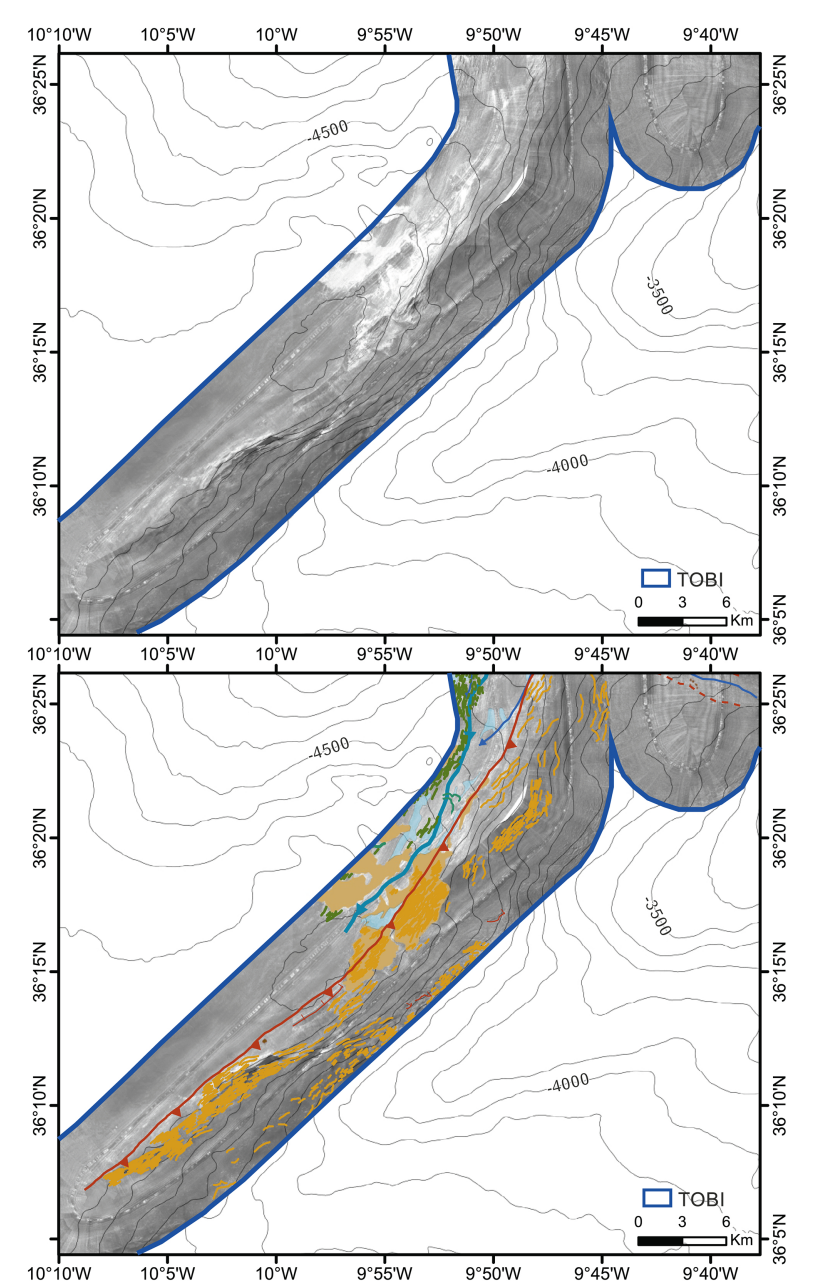
10°10'W
10°5'W
10°W
9°55'W
9°50'W
9°45'W
9°40'W
36°25'N
36°20'N
36°15'N
36°10'N
36°5'N
-4500
-3500
-4000
TOBI
0 3 6
Km

Figure 7

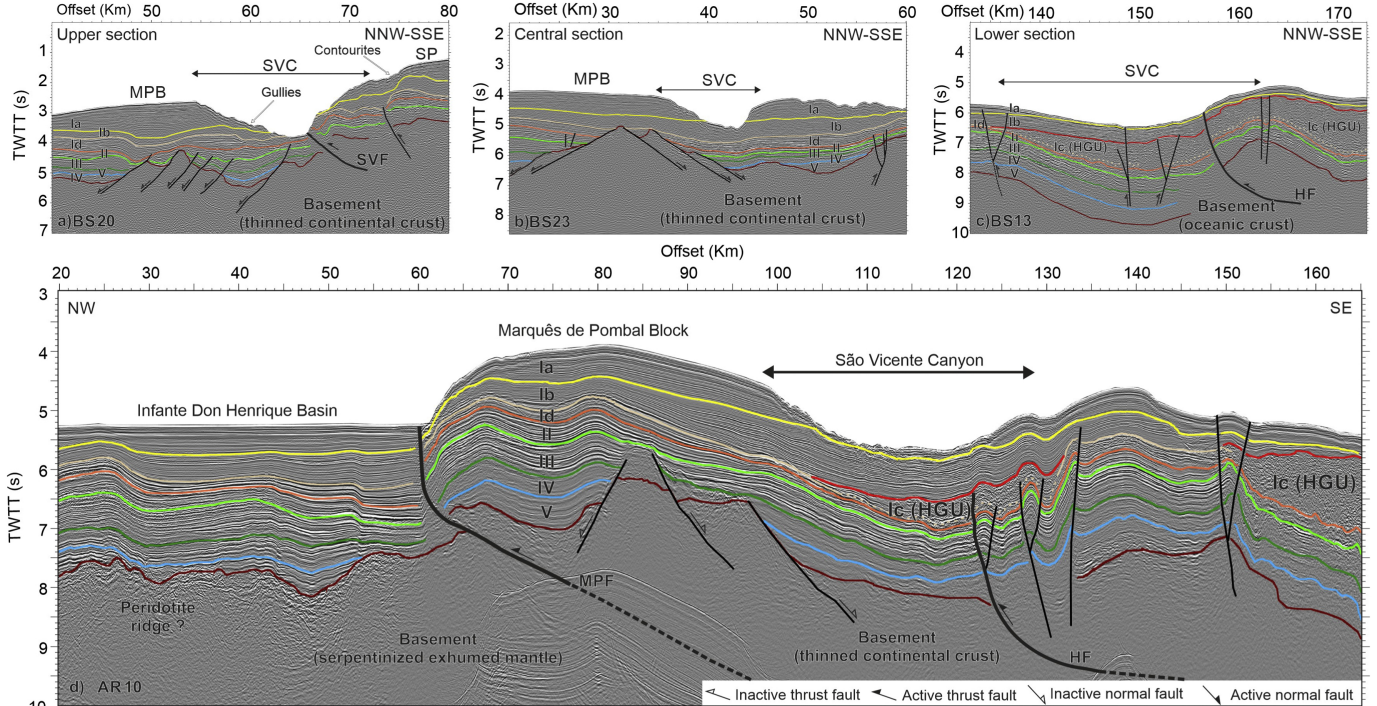
Offset (Km)
Upper section
NNW-SSE
Contourites
SP
SVC
MPB
Gullies
SVF
Basement
(thinned continental crust)
a)BS20
TWTT (s)
Central section
b)BS23
Lower section
Ic (HGU)
HF
Basement
(oceanic crust)
c)BS13
Offset (Km)
NW
SE
Marquês de Pombal Block
São Vicente Canyon
Infante Don Henrique Basin
Ia
Ib
Id
II
III
IV
V
Ic (HGU)
MPF
Peridotite
ridge ?
Basement
(serpentinized exhumed mantle)
Basement
(thinned continental crust)
HF
d) AR10
Inactive thrust fault
Active thrust fault
Inactive normal fault
Active normal fault

Figure 8

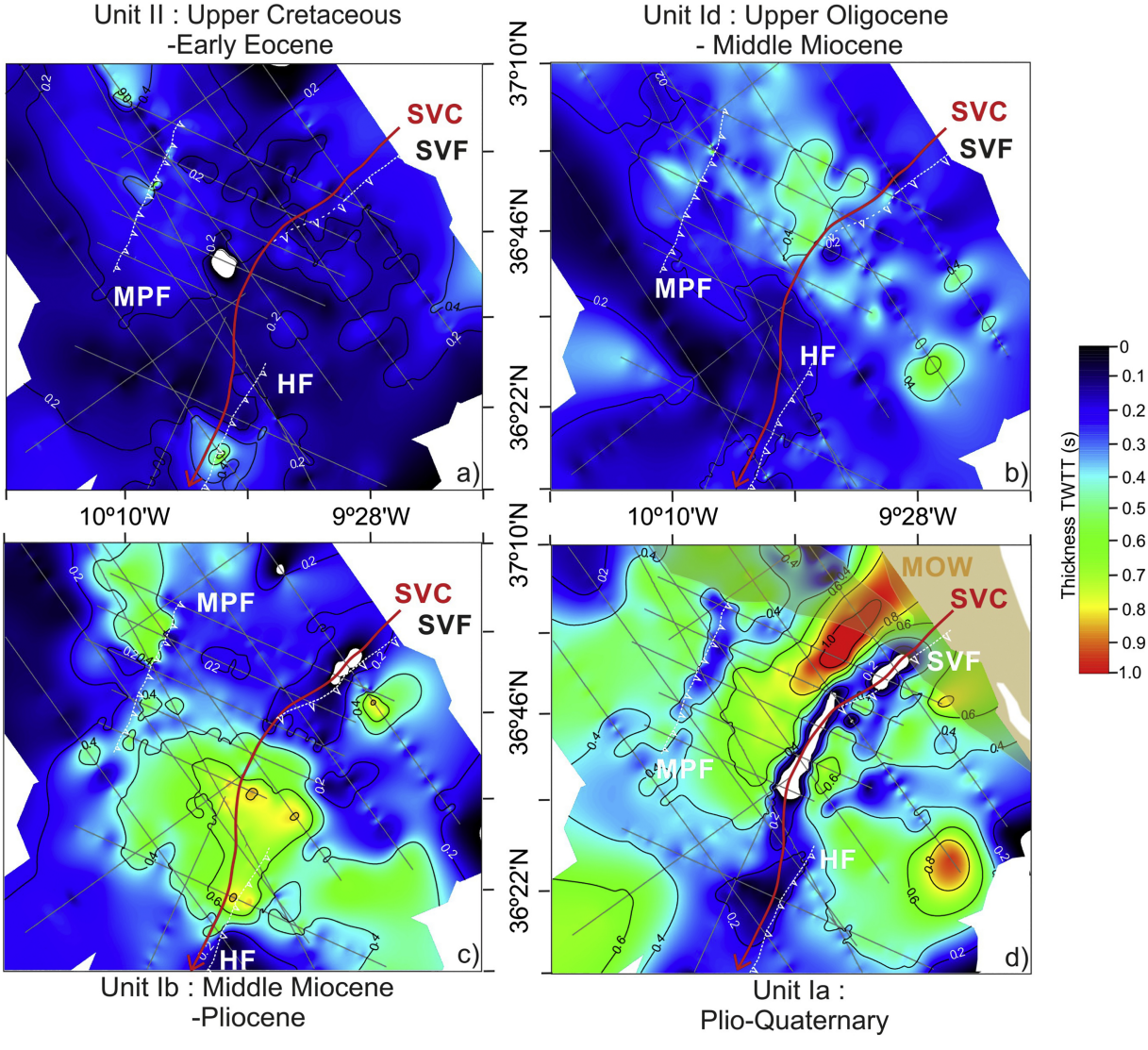
Unit II : Upper Cretaceous
-Early Eocene
Unit Id : Upper Oligocene
- Middle Miocene
Unit Ib : Middle Miocene
-Pliocene
Unit Ia :
Plio-Quaternary
SVC
SVF
MPF
HF
MOW
a)
b)
c)
d)
37°10'N
36°46'N
36°22'N
10°10'W
9°28'W
Thickness TWTT (s)
0
0.1
0.2
0.3
0.4
0.5
0.6
0.7
0.8
0.9
1.0

Figure 9

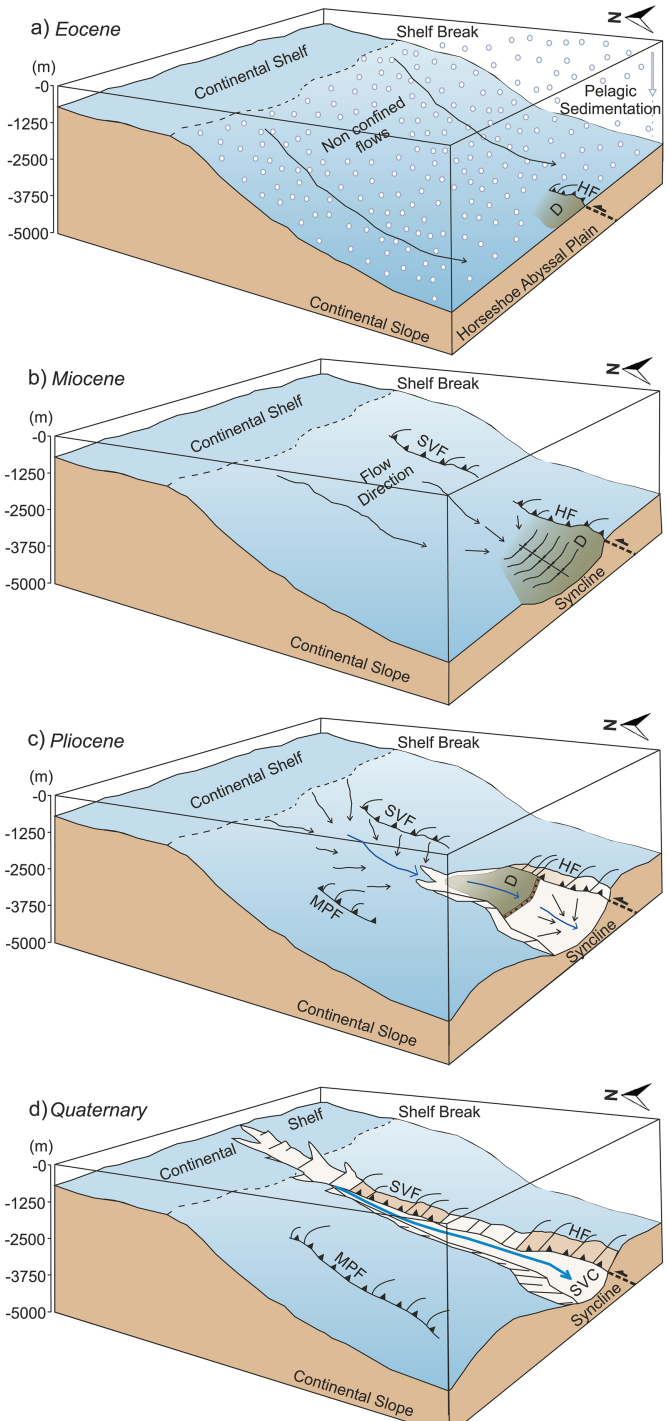
a) Eocene
(m)
-0
-1250
-2500
-3750
-5000
Continental Shelf
Shelf Break
N
Pelagic Sedimentation
Non confined flows
HF
D
Continental Slope
Horseshoe Abyssal Plain
b) Miocene
(m)
-0
-1250
-2500
-3750
-5000
Continental Shelf
Shelf Break
N
SVF
Flow Direction
HF
D
Syncline
Continental Slope
c) Pliocene
(m)
-0
-1250
-2500
-3750
-5000
Continental Shelf
Shelf Break
N
SVF
HF
D
MPF
Syncline
Continental Slope
d) Quaternary
(m)
-0
-1250
-2500
-3750
-5000
Shelf
Continental
Shelf Break
N
SVF
HF
MPF
SVC
Syncline
Continental Slope

Figure 10

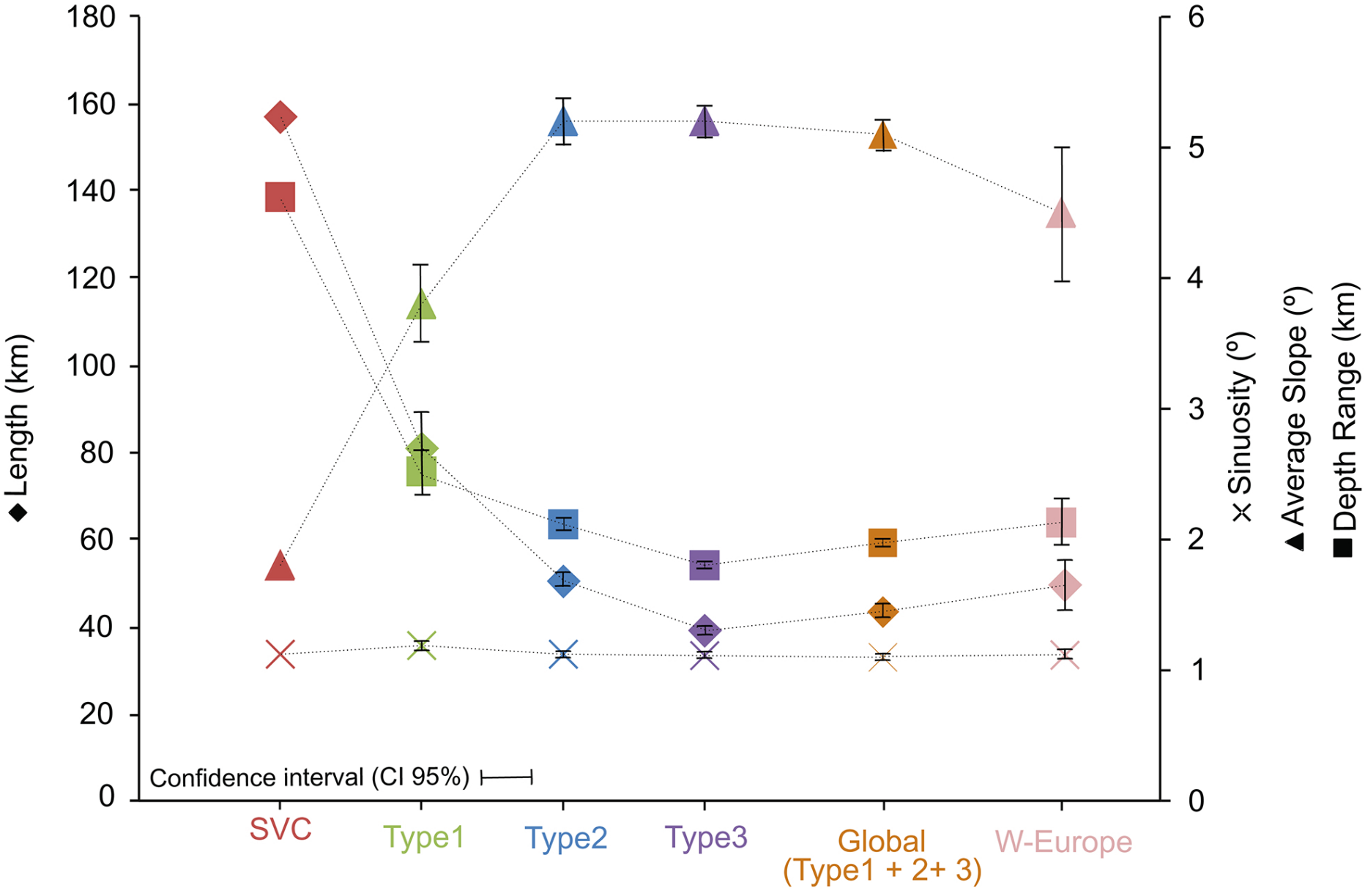
180
160
140
120
100
80
60
40
20
0
◆ Length (km)
6
5
4
3
2
1
0
× Sinuosity (°)
▲ Average Slope (°)
■ Depth Range (km)
Confidence interval (CI 95%)
SVC
Type1
Type2
Type3
Global
(Type1 + 2+ 3)
W-Europe

Figure 11